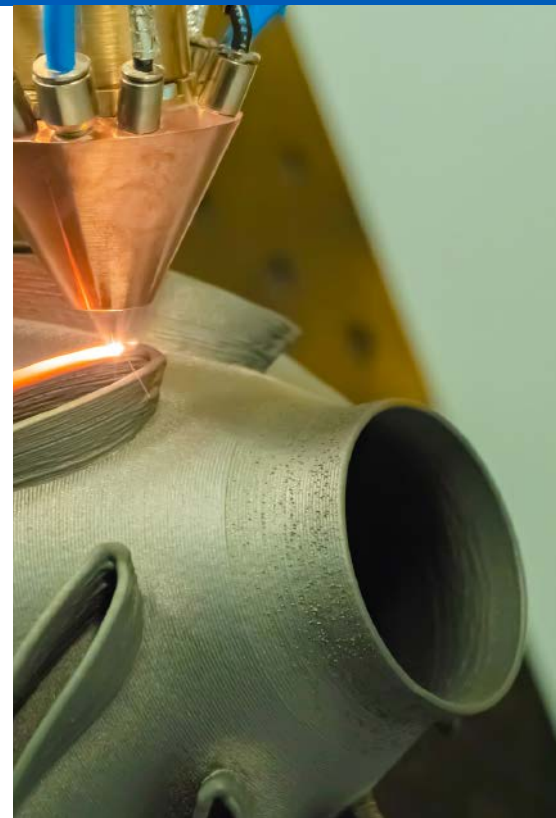


12

Advanced Optical Metrology

Additive Manufacturing:
Metallurgy, Cut Analysis & Porosity



Contents

- 3 Introduction
- 9 Microstructural Porosity in Metal Parts Fabricated by Powder Bed Fusion
- 17 Metal Additive Manufacturing: Design Keys
- 39 Material Parameter Measurement in EVIDENT Microscopy Software Solutions – PRECiV

Imprint

© Wiley-VCH GmbH
Boschstr. 12,
69469 Weinheim, Germany
Email: info@wiley-vch.de
Editor-in-Chief: Dr. Christina Poggel

Additive Manufacturing Process Classification, Applications, Trends, Opportunities, and Challenges

Additive manufacturing (AM), also known as 3D printing, is a process of joining materials to make parts based on data coming from digital 3D models. AM is a layer-by-layer manufacturing process, which differentiates it from conventional subtractive and formative manufacturing technologies.

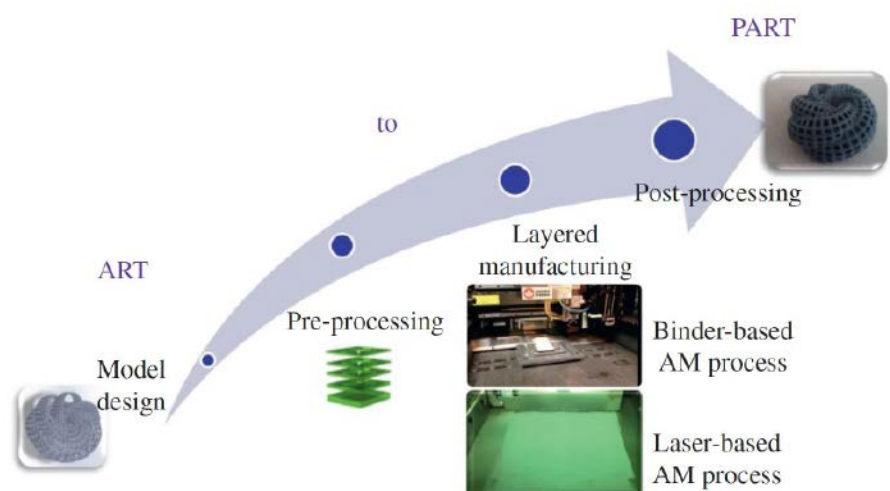
In industry, sector after sector is moving away from conventional production methods to AM, a technology that has been recommended for substantial research investment.^[1] The global economic impact of AM is estimated to be around US\$550 billion per year by 2030.^[2]

Many industries—including aerospace, medical, automotive, tooling, energy, natural resources, consumer, and defense—have started to embrace the benefits of AM. Currently, there is a paradigm shift taking place—for years, AM has been used primarily for customization, prototyping, and low-volume manufacturing. However, in recent years, AM is increasingly being used for mass produc-

tion and is no longer limited to product prototypes. This advancement from prototyping to serial production has created many research and development opportunities, especially for quality management and certification.

The process starts with a digital model that reflects the desired design. Preprocessing is often needed on the file depending on materials, applications, and AM processes. A proper AM process must be chosen that fulfills the material and application of interest. After the layered manufacturing is completed, post-processing may be needed to eventually reach the physical part. **Figure 1** shows the AM process chain schematically.

Figure 1: AM chain producing physical parts from a digital design.



Modern AM started in the 1980s with the ideas of Charles Hull, who successfully acquired a patent for his stereolithography apparatus, a process that solidifies thin layers of photopolymer using a laser beam. Following this concept, many new technologies, including direct metal laser sintering, selective laser melting, and binder jetting (BJ), were developed in the 1990s. The cost of AM machines started to decrease in the 2000s, helping make the technology more accessible and widely adopted. Knowledge of AM concepts, technology, and software are crucial elements of this paradigm shift, and efforts are underway to fully integrate them into educational platforms.

AM CLASSIFICATION

According to ASTM ISO/ASTM52900 standards, AM processes are categorized in the following techniques:

- a. **Binder jetting (BJ):** a liquid bonding agent is selectively deposited to join powder materials.
- b. **Directed energy deposition (DED):** focused thermal energy (e.g., laser, electron beam, or plasma arc) is used to fuse materials by melting while the raw materials are being deposited.
- c. **Material extrusion:** material is selectively dispensed through a nozzle or orifice.
- d. **Material jetting:** droplets of constitutive material are selectively deposited. Examples of materials include photopolymer and wax.
- e. **Powder bed fusion (PBF):** thermal energy selectively fuses regions of a powder bed.
- f. **Sheet lamination:** sheets of material are bonded to form a part.
- g. **Vat photopolymerization:** a liquid photopolymer in a vat is selectively cured by light-activated polymerization.

The industry has adopted PBF, DED, BJ, material extrusion, material jetting, and sheet lamination as the main AM techniques for metal manufacturing, where the mentioned sequence shows the domination of each process in the market.

MAIN ADVANTAGES AND CHALLENGES OF AM PROCESSES

One of the major applications of AM is the manufacture of functional prototypes. Such prototyping usually costs a fraction of conventional processes and is much faster. This accelerates the design cycle (design, test, revision, and redesign). Products, such as molds that would require more than 4–6 months to be developed, can be ready for operation in 2–3 months using AM, making AM an **on-demand, low-cost, and rapid prototyping** tool.

Many time-consuming and expensive manufacturing techniques can be superseded by **fast and efficient** metal AM for **low-volume manufacturing**. However, for mass production, AM still lags behind conventional techniques, such as casting and forging.

One of the most attractive features of AM is that it enables the **fabrication of complex shapes** that cannot be produced by any other conventional manufacturing methods (**Figure 2**). Unlike conventional methods, AM offers a platform for “design for use” rather than “design for manufacture.” Parts with complex or organic geometry optimized for performance may cost less. However, attention must be given to the fact that not all complex parts and geometrical features are manufacturable by AM. Process constraints in metal AM (e.g., overhanging features) may cause issues in terms of residual stresses and defects.

Due to its topology optimization, AM allows the design and manufacture of **high-strength but lightweight structures**, where conventional manufacturing processes fail to do so. This is a highly desirable characteristic in several industries, especially energy and trans-



Figure 2: Complex parts made by AM. The spherical nest has three spheres inside.

portation, because lighter pieces usually mean fewer transport and operating costs.

On the other hand, mechanical assemblies are common in industrial products. Parts consolidation offered by AM provides many advantages due to the reduction of the number of individual parts needed to be designed, manufactured, and assembled to form the final system. AM even removes the need for assembly in some cases. Several applications of AM have obvious benefits for fostering product performance through lightweight/consolidation without compromising high strength, including the optimization of heat sinks to dissipate heat flux better, fluid flow to minimize drag forces, and energy absorption to minimize energy consumption.

The capability to **create multiphase materials** with gradual variations in composition is another important feature of AM. The material composition can gradually be altered to obtain the desired functionality. AM also enables the development of **functionally graded structures** with a single-phase material, where the density gradually changes through the addition of cellular/lattice structures, and embedded objects (e.g., sensors) within structures.

Finally, **prosthetics and implants customized and tailored for specific patients** are already being manufactured using AM. Many developments in the fabrication of soft tissues for the fabrication of organs, as well as a host of other personalized medical items and sensors, are underway. It has been proven

that the use of precise AM replicas can significantly reduce surgery time for many patients.

MARKET SIZE AND FORECAST

The worldwide market for AM hardware, software, materials, and services is anticipated to exceed US\$40 billion by 2027. Moreover, metal AM is one of the fastest-growing segments in the world. The annual growth in the revenue of metal AM materials has been higher than that of photopolymers, polymer powders, and filaments between 2013 and 2018.^[3] The systems that were dominant in the market of metal AM include PBF (mainly with a laser heat source) and powder-fed laser DED as well as new technologies, such as BJ and cold spray. Most material sales include metal powders and wire feedstock.

In terms of market share, the aerospace industry covers the largest share, followed by the medical sector.^[4] The aerospace industry profits from turbines, helicopters, and jet-engine component fabrication as well as new space applications such as rocket engines, attracting large venture capital worldwide, especially in the United States.

METAL ADDITIVE MANUFACTURING APPLICATIONS

AM processes began adapting to different sectors as early as 1990, as shown in the timeline in **Figure 3**.

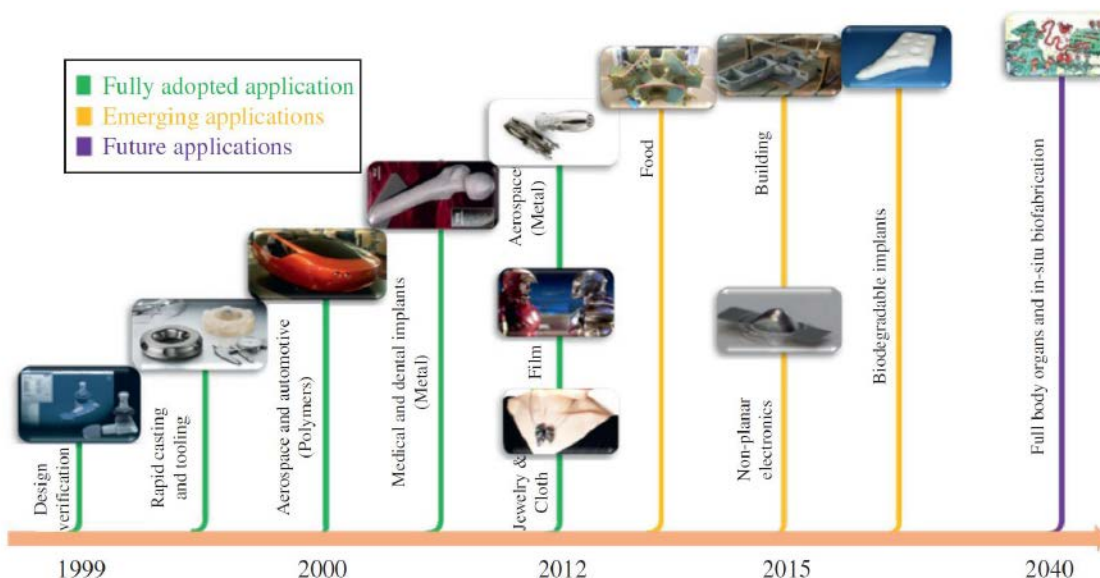


Figure 3: Timeline for adopted, emerging, and future applications of AM.

Figure 4 schematically shows three classes of AM processes (PBF, BJ, and DED) widely employed in metal manufacturing. For large-size components, the powder-fed and wire-fed DED processes are the most applicable, where the printed part may not require high resolution with complex features. In contrast, PBF and BJ can be used for smaller metal parts with higher resolution and complexity. In contrast, the density of parts produced by DED is almost perfect, but in BJ, the density cannot be high. PBF is a middle process that can produce relatively large parts up to 50 cm with high resolution and high complexity using the current state of PBF technology since 2020.

The **medical industry** was one of the early adopters of AM for the fabrication of not only metal parts, but also ceramics, polymers, and functionally graded materials. Metal AM has been used to produce medical devices and tools, surgery guides and prototypes, implants, prosthetics, orthotics, dental implants, crowns, and bridges from biocompatible metals, such as various titanium, tantalum, and nickel alloys. Due to the high precision required to produce medical parts, PBF processes are the dominant AM technique in this sector. In addition, porosity and selective stiffness are of major importance to medical devices. Thus, BJ is playing an important role as it can produce implants with controlled porosity.

AM is also particularly attractive in the **aerospace and defense industries** because the lower material waste, light weight, reduced need for assembly through component consolidation, and the capabil-

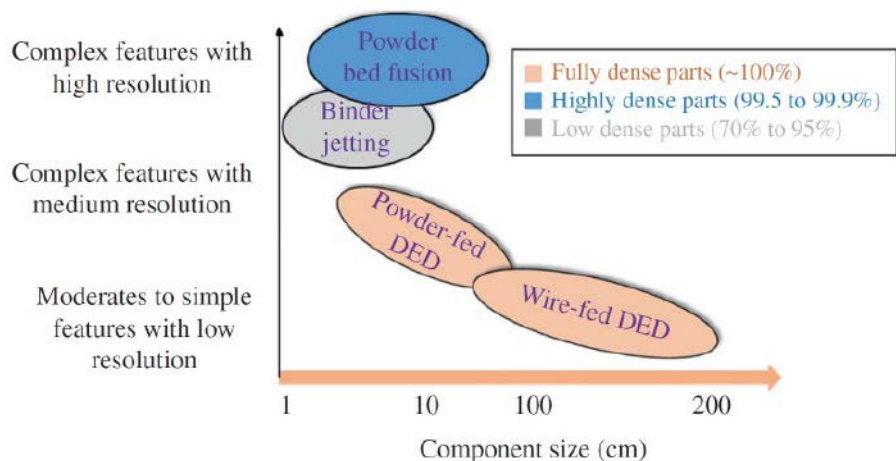
ity to produce highly intricate and complex parts contribute to cost savings and lower fuel consumption thanks to a lower level of certification required for fewer parts.^[5]

In space applications, the race is even faster paced. In 2015, the first-ever communications satellite with a design life of 16 years and weight of 4.7 metric tons (named TurkmenAlem52E) with an aluminum 3D printed antenna horn mounting strut was launched by SpaceX. On the rocket engine applications, major activities are underway by SpaceX, NASA, and Aerojet Rocketdyne to adopt AM for rocket engine components because the qualification testing and heritage could be transferrable in many situations.

DED technology is also used in the aerospace and defense industries for repairing and refurbishing parts. It is a particularly important application given the long life cycle of aviation systems and the high cost and long lead-time associated with the replacement of the parts.

Additionally, AM processes can enable the manufacture of complex-shaped metal and plastic antennas from different alloys and dielectrics, opening up tremendous opportunities for the **communication industry**. Advanced AM-made RF antenna structures have the potential to revolutionize the design, supply, and sustainment of such devices. An AM design process can be fully integrated into the antenna design platforms to support not only customization but also antenna performance enhancement in the field.

Figure 4: Most important metal AM processes versus part size, complexity, and resolution needed.



The rapid prototyping feature of AM provides a key step in the design verification to attain innovative solutions in the **energy and resources industries**. AM has also become an increasingly mainstream operation to fabricate end-use functional parts at a low-volume level. When AM-made parts need tooling, it can be used to make lightweight structures with complex internal features. Thus, the next generation of energy, oil, and gas components have substantially benefited from AM features, especially parts that need to meet performance and environmental standards. Dense, corrosive-resistant, and high-strength components can be developed using DED for demands in the energy and resources industries. One crucial application of AM in these industries is the development of spare parts.

The application of metal AM in the **automotive industry** has been in the creation of prototypes, heritage parts for obsolete models, and spare parts and tools. Even though the automotive industry is not yet using AM directly for the production of final metal parts in serial production vehicles, a new trend for reaching that goal has already started. Many automotive companies such as Volkswagen, BMW Group, Porsche, General Motors (GM), and Toyota have entered the AM market either through investing in the improvement of their in-house AM capabilities or through making alliances with machine developers, 3D software companies, AM material producers, or research centers to expedite the adoption of metal AM.

Finally, one of the obvious applications of metal AM is in **tooling** and **mold production** for other industries, such as medical, aerospace, and automotive. In the consumer products sector, the promise of mass customization drives the gradually increasing usage of metal AM in various consumer products, such as decorative objects, jewelry, custom sports gear, and structures (bicycle frames). The design freeform, material graded structures, light weight, and fast design-to-market cycle offered by AM are predicted to have revolutionary effects on industrial and personal products.

ECONOMIC AND ENVIRONMENTAL BENEFITS AND SOCIETAL IMPACT

AM technologies are usually greener than conventional methods because there is less material wasted, and there may be up to 50% energy savings during part production.^[6]

Moreover, metal-based AM technologies virtually eliminate machining and the subsequent need for toxic cutting fluids as well as costly pollutants that are challenging to dispose of and have a negative environmental impact.^[7] In addition, AM parts can reduce weight in the range of 50–100 kg per aircraft, significantly reducing fuel costs; every kilogram removed from a fleet of 400 commercial jet-liners leads to an annual fuel consumption reduction of 60,000 L (15,850 gallons).

When machining a block of material for simple geometries would be preferable, AM will be much more appealing for making parts with hollow shells, lattices, features with complex curvatures, and internal conformal channels. Thus, AM's sustainability is correlating with geometric complexity. It is important to do a thorough analysis of the sustainability of metal AM upfront to understand the benefit of the process for a specific geometry. In addition, life cycle assessment studies are needed to quantify the environmental impact of AM more precisely. The full product life cycle from production to overhaul must be included in the analysis.

AM TRENDS, CHALLENGES, AND OPPORTUNITIES

In addition to new business models being developed by various industries, there are several challenges that the AM community must overcome:

- a. **Qualified materials:** one of the major challenges in the field of metals and metal alloys is the number of powders that have been qualified for use with metal AM systems, including laser, electron beam, and binder-based AM processes.
- b. **Speed and productivity:** further process development is needed to enhance surface quality during AM processes to improve speed and productivity.
- c. **Repeatability and quality assurance:** AM is sensitive to both environmental and process disturbances, from fluctuating temperature and humidity levels to non-uniform powder sizes. Full control of the process and surrounding environment is difficult, so there's a focus on solutions that employ sensors to monitor conditions and quality control algorithms to automatically adjust process parameters—such as laser power and process speed—through closed-loop control systems to compensate for any disturbances.

- d. **Industry-wide standards:** the absence of such standards may hinder the continued adoption of AM for industrial applications.
- e. **End-to-end workflow, integration, and automation:** many customers are reluctant to accept a new material/process/design or technology that does not have history in their applications. To minimize industry hesitation on AM adoption, an effective end-to-end workflow must be developed that is simple yet integrated and automated. Currently, the lack of digital infrastructure is a major obstacle to creating effective automated workflows for the AM industry. Automated AM is part of the factory of tomorrow, a forefront of the ongoing industrial revolution within the industry 4.0 approach.
- f. **Software limitations:** commercially available software for designing AM parts, support structure development, and interfacing with AM machines have limitations in assessing the feasibility of prints and identifying process constraints. The current software and hardware still need more improvements to facilitate timely communication in AM.
- g. **Initial financial investments:** the AM ecosystem covers software, materials, experts, post-processing equipment, certifications, as well as training for employees. This investment can be large, hindering companies from embracing this technology effectively.
- h. **Security:** AM has promoted globally distributed manufacturing, and the existence of hackers is a reality. They can tweak the AM designs to create intentional defects that are not detectable but may have catastrophic consequences when used in actual systems.
- i. **Skillsets gap:** there is a limited workforce of qualified personnel that can develop an entry strategy for companies that want to embrace AM. Overall, learning about the capabilities and limitations of metal AM will aid companies in developing meaningful and successful applications for the technology. Promoting AM consultancies is another way to foster knowledge transfer. In addition, AM conferences and webinars are playing critical roles to fill the skillsets gap.

As these challenges are overcome, AM will transform the entire manufacturing sector over the next 10 to 15 years. With AM, designers do not design for manufacturing anymore—they design for end-users. This is a paradigm shift. Finally, it is reported that AM would be able to reduce the capital required to reach a minimum manufacturing volume.^[8]

REFERENCES

- [1] C. A. D. Competitive, A. In, and A. Manufacturing, "Executive Office of the President President 's Council of Advisors on Science and Technology," 2012. [Online]. Available: https://www.energy.gov/sites/prod/files/2013/11/f4/pcast_annex1_july2012.pdf
- [2] J. Bromberger and K. Richard, "Additive manufacturing: A long-term game changer for manufacturers," McKinsey Co., 2017. [Online]. Available: <https://www.mckinsey.com/business-functions/operations/our-insights/additive-manufacturing-a-long-term-game-changer-for-manufacturers>
- [3] T. Wohlers, *Wohlers Report 2020: 3D printing and additive manufacturing state of the industry*, Wohlers As. Wohlers Associates, 2020. [Online]. Available: <https://www.wohlersassociates.com/2020report.htm>
- [4] "AMPOWERreport, 'Metal additive manufacturing suppliers predict a market size growth of 27.9%.'" [Online]. Available: <https://additive-manufacturing-report.com/additive-manufacturing-market>
- [5] J. O. Milewski, *Additive Manufacturing of Metals*, vol. 258. Cham: Springer International Publishing, 2017. doi: 10.1007/978-3-319-58205-4.
- [6] DOE-ADVANCED MANUFACTURING OFFICE, "Additive Manufacturing : Pursuing the Promise," Doe, p. 2, 2011, [Online]. Available: https://www1.eere.energy.gov/manufacturing/pdfs/additive_manufacturing.pdf
- [7] N. Diaz, M. Helu, S. Jayanathan, Yifen Chen, A. Horvath, and D. Dornfeld, "Environmental analysis of milling machine tool use in various manufacturing environments," in *Proceedings of the 2010 IEEE International Symposium on Sustainable Systems and Technology*, May 2010, pp. 1–6. doi: 10.1109/ISSST.2010.5507763.
- [8] B. Mcgrath, "3D opportunity for life cycle assessments. Additive manufacturing branches out," *Deloitte Univ. Press*, p. 20, 2015, [Online]. Available: https://www2.deloitte.com/content/dam/insights/us/articles/additive-manufacturing-in-lca-analysis/DUP_719-3D-opportunity-life-cycle_MASTER.pdf

01 Microstructural Porosity in Metal Parts Fabricated by Powder Bed Fusion

A. Sola, A. Nouri

ABSTRACT

Metal additive manufacturing (AM) is a manufacturing technique that can build complex metal parts layer by layer. Powder bed fusion (PBF) is one of the most common AM techniques. However, PBF induces microstructural defects that can adversely affect the performance of the manufactured components. The present article provides an overview of the formation mechanisms of pores in AM metals and some emerging techniques for the detection and quantification of pores.

INTRODUCTION

Additive manufacturing (AM) is the most appropriate definition that reflects the use of the layer-by-layer addition of material to build up 3D objects. The AM fabrication process includes two basic steps: coating and consol-

idating. The coating step requires applying a new layer of material to the existing working surface. While the consolidating step implies printing the newly applied layer to the underlying layer using sintering, melting, polymerizing, or other processes. The consolidating step is carried out by an energy source, which can be a light beam or an electron beam. The two steps, coating and consolidating, are repeated layer by layer until the full part is produced.^[1]

AM offers unmatched flexibility with respect to the part geometry;^[1-5] however, surface roughness and waviness of AM parts are one of the main disadvantages of these methods that must be mitigated through surface finishing technology in order to enhance component performance.

Powder bed fusion (PBF) is one of the most commonly used AM techniques. PBF requires powdered feedstock that is sequentially processed in thin layers and solidified either by a laser beam (L-PBF) or by an electron beam (EBM).^[6]

A schematic illustration of an L-PBF instrument setup is shown in **Figure 1**. Upon moving down the build platform, a new layer of powder is deposited on top of the pre-

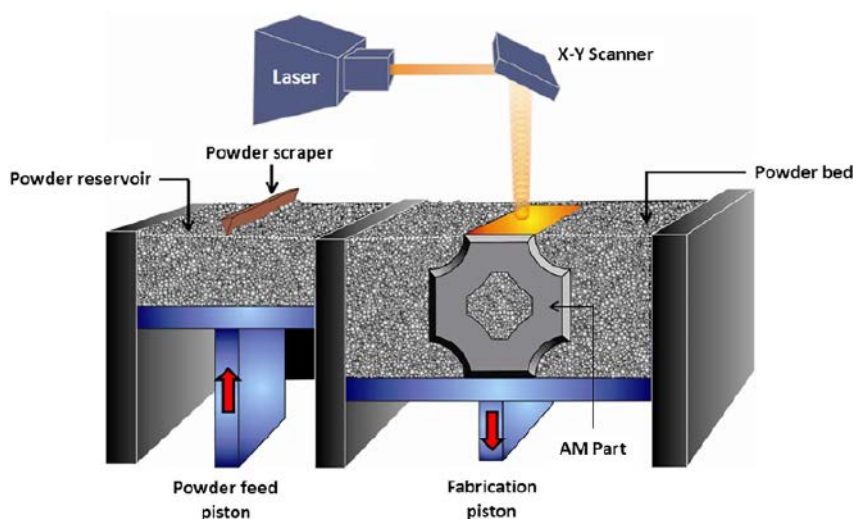


Figure 1: Schematic representation of laser-based powder bed fusion process and equipment.

vious layer, and the procedure is repeated until the complete object is produced. The energy conveyed by the laser beam is high enough to also reach the previously consolidated layers that are partially re-melted or re-sintered together with the new powder. In this way, interlayer bonding is obtained.^[7]

With respect to other AM methods, L-PBF takes advantage of processing a wide variety of powder materials.^[7,8] Powders that are not likely to melt or sinter can also be processed via L-PBF by adding a sacrificial binder material, typically a polymer binder. The binder is removed afterward using thermal treatment (debinding); however, a further post-processing step is required to reduce the residual porosity, which can be as high as 60%. Thus, almost fully dense parts can be obtained by either post-processing via furnace sintering, hot isostatic pressing (HIP), infiltration with a polymer, or with a low-melting-point metal^[7]. On the other hand, EBM is only applicable to conductive materials (i.e., metals) and is used preferentially for titanium alloys^[9].

Regarding the disadvantages, pores and voids are reported to be the most frequently occurring defects in selective laser sintering (SLS).^[10] In addition, a variety of microstructural inhomogeneities may also be present in PBF parts, including impurities (inclusions, contaminations, and metal oxides), not melted or partially melted particles, and anomalous grain growth and crystallographic textures.

In this article, the term “pore” is used to refer to microstructural pores, defined as residual voids and defects in the microstructure of the built part.^[46] They are formed unintentionally and must be avoided or minimized to limit their adverse effect on mechanical properties and to ensure the consistency of AM parts.

FORMATION MECHANISMS OF PORES IN DIFFERENT METAL PARTS

Steel and other ferrous alloys

Khairallah et al.^[11,12] proposed a model to simulate the melt-flow mechanisms and their impact on the microstructure of 316L stainless steel processed by L-PBF. According to the model, as the laser scans over the powder bed, an indentation is created and subsequently collapsed due to an abrupt reversal of the melt-flow velocity-vector field. This sudden breakdown of the depression favors

the entrapment of gas bubbles at the bottom of the track. The abrupt change in the velocity-vector field also results in the formation of a vortex that further promotes the development of bubbles and the eventual coalescence of such bubbles into a larger pore. In L-PBF, if the balance of the laser power, scan speed, and beam size exceeds a threshold value, the melting mode is controlled by evaporation (keyhole mode). The resulting melt pool is no longer semicircular, and the laser beam can affect the metal down to a deeper depth than in the more-common conduction mode. Due to the repeated formation and collapse of vapor cavities, a sequence of voids is created along the laser beam path.^[13,14] This model is able to explain the formation of additional pores other than keyholes. In the transition zone of the melt track, occasionally, the quick movement of the laser beam does not allow for the complete melting of the particles at the rim of the track. Particles that are not properly melted cannot be incorporated into the melt pool and the voids between them cannot be filled.

Choo et al.^[15] fabricated 316L stainless steel parts by L-PBF under decreasing power levels. As a consequence of decreasing laser power, porosity was initially increased due to an increase in the number of pores, whereas the average pore volume remained unchanged. With a further decrease in laser power, porosity continued to increase due to the increase of the average pore size, whereas the number of pores slightly decreased. In fact, when the energy input became insufficient to enable complete melting of the feedstock or to induce an effective overlap between adjacent scan tracks, the frequency of pores and the lack of fusion defects progressively increased. In the end, pores and defects could link and coalesce, resulting in a reduced number of large and flat pores that were preferentially perpendicular to the growth direction. Moreover, independently of the laser power, large spherical pores with keyhole geometry were preferentially distributed at the edge of the samples, where the scan tracks came to an end or changed direction due to the scanning strategy as previously observed also by Khairallah et al.^[11,12]

Åsberg et al.^[16] processed a tool made with steel H13 using L-PBF and investigated the effect of different thermal treatments on residual porosity. The level of porosity was higher near the edges than in the core of the cross-section. Such subsurface porosity could be associated with the change from core scanning strategy to contour scan-

ning strategy, where the speed and direction of the laser beam are changed.^[11,12,15] Stress relieving heat treatment alone or combined with standard hardening and tempering treatment did not cause any change in porosity, whereas HIP induced sensible densification by closing the lack of fusion defects and reducing the size of gas pores.^[16]

Morrow *et al.*^[17] investigated 304L and 316L stainless steel gas atomized powders and underlined the importance of the chemical composition and morphological aspects of feedstock powders. Furthermore, the presence of nanoscale particles that cause submicron precipitates in the finished parts and gas entrapment is likely to outlive L-PBF processing.

Titanium and its alloys

Gu *et al.*^[18] analyzed the effect of different scanning speeds on the microstructure and related mechanical properties of commercially pure titanium (cp-Ti) parts produced by SLM. Considering the mechanical behavior, the SLM parts processed at low scan speed exhibited relatively low values of hardness and wear resistance. The limited performance of these samples was related to the presence of thermal cracks, and also to the development of coarsened grains. For a very high scan speed, the formation of a refined martensitic phase was favored, but the mechanical properties were equally diminished due to the presence of balling-induced large defects.

Cunningham *et al.*^[19] applied advanced synchrotron-based X-ray microtomography to analyze the presence of pores in EBM Ti-6Al-4V parts both in the as-built and post-processed HIP state. As-built parts were affected by spherical and irregular pores. The presence of pores in the feedstock powder was shown to correspond to the presence of spherical pores in the as-built components. Alternatively, irregular pores were mainly formed due to a lack of fusion. After the HIP treatment, they observed that only the irregular pores caused by lack of fusion were eliminated, while the spherical pores that were initially formed by gas entrapment in the feedstock powder survived.

Thijs *et al.*^[4] performed a systematic analysis of the effect of processing parameters and scanning strategy on the microstructure of Ti-6Al-4V parts processed by SLM. When the laser scanning velocity deviated from its optimal value, the part density suddenly dropped due to the formation of large, elongated pores alongside the scanning direction.^[4]

Qiu *et al.*^[20] reported that when the layer thickness was kept constant with a relatively low value (= 20 μm in their study), the porosity of Ti-6Al-4V parts processed by SLM became lower with increasing laser power and scan speed. However, if the scan speed is excessively increased and the laser power is not adjusted accordingly, the pores are expected to develop due to the low energy density and the resulting lack of fusion. The observed porosity could be closed almost completely by the HIP. However, the complete elimination of porosity after HIP was not the only reason for the improvement in ductility and loss in strength since the martensitic phase originally present in the as-built part was also transformed into α and β phases.^[20]

Aluminum alloys

Processing Al alloys pose additional problems with respect to steel and Ti alloys, due to the strong reflectivity of Al-based powder, its high thermal conductivity that quickly disperses heat from the melt pool to the previously consolidated layers, and the possible formation of oxides on top of the melt pool^[21]. As a result, even if almost fully dense Al-based parts can be produced by SLM, various mechanisms can induce the formation of voids^[2,3,5,21]. Some of these mechanisms are related to the feedstock powder and some are related to the processing conditions.

Weingarten *et al.*^[5] found that any attempt to increase the build-up rate by increasing the laser beam diameter or the powder layer thickness can cause a density loss as high as 10%. This is mainly a consequence of the gas porosity that remains entrapped in the metal due to the fast processing condition and rapid cooling.

The importance of surface moisture was also emphasized in A357 parts processed by SLM.^[22,23] The existence of very small spherical pores with a diameter smaller than 5 μm was equally attributed to the presence of moisture on the surface of feedstock particles and the reactions with Al. Despite the initial small size of the hydrogen-rich pores, they were sensibly enlarged during high-temperature solution heat treatment.

According to Tang and Pistorius,^[24] the fatigue life of AlSi10Mg parts produced by SLM is drastically reduced by pores associated with small oxide fragments that form from the Al oxide film on the feedstock powder. Unlike the Al alloy, the Al oxide film does not melt during SLM processing. Since the wettability of melted Al-Si alloys toward Al oxide is very

low,^[25] the melted metal inside the particle separates from the native oxide film on the surface. The oxide film is very thin and brittle and is likely to break and generate submicron fragments.^[24] Tang and Pistorius^[24] also observed a correlation between large pores and coarse oxide particles and fragments. Since the melted Al-Si alloy is not able to wet oxides, the presence of large oxide particles adversely affects the consolidation mechanisms. Such large defects were concentrated on the upper part of the constructs, suggesting that oxide particles are preferentially developed close to the top surface or are moved up there through vaporization and spatter mechanisms.^[24]

Similar to other metal AM parts, in Al alloy components the presence of not melted particles and oxides is also expected to cause porosity with a random geometry.^[21] Thijs *et al.*^[21] observed large and elongated keyhole pores that were preferentially located near the edge of parts (i.e., at the start/end points of the scan tracks) where heat is likely to accumulate.

Coherent results were presented by Romano *et al.*,^[26] who underlined the combined effect of size and location of pores. As a rule, a surface defect is more detrimental to fatigue life than an embedded pore with the same size and shape. In fact, a surface defect was proven to cause a 30% larger stress intensity factor than an embedded defect.

Nickel-chromium (Ni-Cr) superalloys

Sheridan *et al.*^[27] analyzed the effect of scan strategy (movement pattern of the laser beam) and processing parameters on the formation of porosity in Inconel 718 parts processed by SLM. The continuous scan strategy (a continuous meandering movement of the laser beam) resulted in a lower average density of pores and a lower size distribution of pore population with respect to the striped and island-based scan strategies. An appropriate setting of the processing parameters, including laser power, scan speed, hatch spacing, and layer thickness allowed to reach fully dense parts. Notably, the potential effect of pores on fatigue life depends on their relative distance from each other, their distance to the surface, and their location with respect to crystallographic features, such as grain boundaries and triple or quadruple joints.^[28]

POROSITY DETECTION AND MEASUREMENT

Two different approaches to porosity analysis are proposed in the literature. The first one is a post-processing strategy (detecting, measuring, and possibly analyzing the existing pores in the finished part). Alternatively, the development of pores can be evaluated in situ, directly during manufacturing; in this way, if problems arise during manufacturing, the printing parameters can be corrected at an early stage, typically through closed-loop repairing tactics.^[29]

Post-processing detection of porosity

Porosity, P , has often been estimated from the measurement of density, through the equation:

$$P = \left(1 - \frac{\rho_{\text{measured}}}{\rho_{\text{theoretical}}}\right) 100 \quad (1)$$

Where ρ_{measured} is the measured density of the part and $\rho_{\text{theoretical}}$ is the theoretical density of the fully dense material. This technique is not able to account for those cavities that are filled with not melted particles. In addition, if Archimedes' principle is used, the density measurement is significantly affected by the surface roughness.^[6,30] Moreover, unlike conventional wrought materials, $\rho_{\text{theoretical}}$ is not certain for powders and parts in AM, since their exact chemical composition can be altered by feedstock recycling and possible preferential evaporation of elements during alloying processing.^[31] This method may be used to quantify the volume fraction of pores (within the limits previously discussed), but it is not able to provide any information about the size, morphology, and distribution of pores within the part.

Cut and polished cross-sections can be used for direct observation under optical and electron microscopes. However, the metallographic preparation is likely to introduce artifacts and significant morphological changes. Moreover, the result may be biased by several parameters that are arbitrarily chosen. Automatic image analysis strategies are nowadays the focus of research in order to overcome the arbitrariness associated with human error.^[31] Micro-computed tomography (micro-CT) is a nondestructive technique that preserves the integrity of tested samples and enables the repeated execution of the test on the same part at different stages of its processing history, for example, before and after HIP.^[15,32,33] The main advantage of micro-CT is the possibility of examining the shape of pores and their spatial distribution in three dimensions. However, high-quality images can only be obtained

if two conditions are satisfied. First, the X-ray absorption of the constituent phases in the sample must be different. Next, the transmitted X-rays must preserve at least 10% of their original intensity. To this aim, if necessary, smaller samples are to be cut from the originally built part. In this case, micro-CT can no longer be considered a non-destructive technique.^[15,34] Furthermore, the accuracy of pore detection is affected by the resolution limit of the tomography equipment, which depends on the voxel size^[31] and on the thresholding strategy applied to separate noise and the objects that should be identified as pores.^[33]

In situ monitoring of pore formation

Process signatures (critical quantities that are measured in situ) are dynamic quantities that relate to the powder during heating, melting/sintering, and solidification. They can be grouped into either observable signatures or derived signatures.^[12]

Most of the available in situ monitoring systems are based on contactless temperature measurement, imaging in the visible range, and low-coherence interferometric imaging. Sensors can be aligned along the optical path of the laser beam (i.e., coaxial configurations); otherwise, they work at a given angle of view outside the optical path (i.e.,

off-axial configurations). Coaxial configurations are only compatible with L-PBF because the electron magnetic coils that are necessary to direct the electron beam in EBM do not permit the presence of coaxial sensors.^[29]

The progress in sensing equipment must be supported by adequate computational means to store and manage the huge amount of data acquired in situ.^[29] Effective feedback and reactive or corrective systems are still the subjects of much scientific research.^[29]

DISCUSSION

Recently, Zhang *et al.*^[35] reviewed pores and other defects in SLM and classified them into three groups: (a) porosities, which are mainly spherical and less than 100 μm ; (b) melting-related defects, which are characterized by irregular shape, and (c) cracks, which are the result of quick cooling, sharp thermal gradients and thermal stresses.^[35] A schematic representation of these pores is seen in **Figure 2**.

Defect formation mechanisms can be broadly categorized into equipment-related, powder-related, and processing-related defect formations:

a. Equipment-related defect formation:

it is evident that the high scanner deflection angles at the edges of the baseplate induce an elliptical distortion of the laser spot, which may cause porosity and lack of fusion in L-PBF.^[29] Ferrar *et al.*^[36] also reported on the possible formation of pores associated with the inefficient flow of the inert gas through the build chamber. For example, the equilibrium partial pressure of oxygen at the melting point of Ti should be less than 10^{-16} atm to prevent oxidation, which is infeasible from a practical point of view. As a consequence, a certain degree of defectiveness, which includes balling and lack of interlayer bonding, is inevitable.^[25]

b. Powder-related defect formation: the powder flowability affects the feeding efficiency, whereas its compressibility determines the particle density within each newly applied powder layer.^[37] Absorbed soluble gasses (especially, hydrogen) are also potentially harmful because they can be released during AM processing. Surface-absorbed moisture is believed to be a potential source for hydrogen-related defects in Al alloy parts. Pores and spatter formation are also facilitated by feedstock powder oxidation because

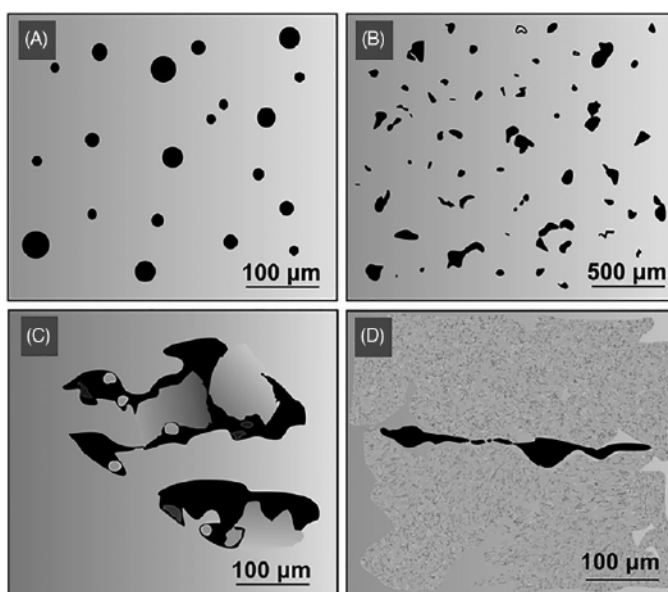


Figure 2: Characteristic pores in laser-based powder bed fusion parts: (A) entrapped gas porosity; (B) incomplete melting-induced porosity; (C) lack of fusion with not melted particles inside large irregular pores and (D) cracks.

of powder handling, reuse, or prolonged storage in an unsuitable environment.^[38]

c. Process-related defect formation: if the laser power is too low or if the scan speed is too high, lack of fusion results in not melted particles, and hence the newly added powder layers become increasingly uneven with irregular cavities filled with loose or inadequately fused particles.^[9,39,40] If the laser power is too high or the scan speed is too low, conversely, keyholing is highly probable.^[11,12] The powder layer thickness is also a key parameter: if the layers are too thin, overheating may occur; on the other hand, if the layers are too thick, interlayer bonding is not effective.^[9,40] Thermal residual stresses are another source of microstructural defects. The thermal mismatch generates residual stresses that cause cracking.^[41] Although the appropriate selection of the processing parameters results in almost fully dense parts (with densities exceeding 99.5%), the surviving pores unavoidably impair the mechanical properties of AM parts, especially under tensile and fatigue loading.^[41]

Some post-processing treatments have been proposed to reduce the residual porosity in AM parts. While HIP appears to be the most effective treatment, it fails to eliminate trapped gas bubbles.^[19] Additionally, the high temperatures reached during HIP may result in some adverse effects, such as grain coarsening or phase transformation.^[42,43] Surface finishing is often applied to reduce surface roughness and possibly to reduce superficial defects that are likely to diminish fatigue resistance. However, in the case of subsurface porosities, surface finishing brings such defects to the surface and these emerged pores become potential crack initiation sites for fatigue failure.^[44]

According to the available literature, three main hurdles are yet to be overcome to control and minimize the formation of pores in PBF parts:

1. First, the determination of the pore volume fraction is the minimum requirement. However, the morphology, size, and distribution of pores are also playing an important role in several applications.
2. After identifying the most appropriate characterization technique, the sensitiv-

ity of the available instrumentation should be considered with respect to the critical size of the defect for a given application.

3. Additionally, since the unexpected appearance of pores may be a sign of production anomalies, particular attention should be paid to in situ detection systems. The detection of potential anomalies is particularly challenging since AM methods inevitably imply stochastic fluctuations and are often applied to the production of one-of-a-kind parts, which do not have standards for comparison purposes.^[6,45]

CONCLUSIONS

Despite the stochastic nature of PBF techniques, a survey of the available literature reveals that some recurrent mechanisms cause the development of microstructural pores. Basically, pores can outlive into the finished parts from the feedstock powder through the gas entrapment during the gas atomization process. Pores may also have originated from the presence of moisture on the surface of the feedstock particles. Alternatively, pores can be originated from an improper setting of the processing parameters.

Moreover, additional process conditions such as the scan strategy may affect the porosity of the finished part. The pre-treatment of the feedstock to remove the surface moisture, as well as the optimization of the process parameters, can be applied to reach density values higher than 99.5%. The residual presence of pores significantly affects the mechanical behavior, especially fatigue life, of the finished parts. As a consequence, the debate is now open in the literature on two basic requirements, namely a further reduction of the residual porosity and the development of appropriate means to detect the formation of pores and microstructural defects in situ. The achievement of these two goals can significantly contribute to the future industrial development and advancement of PBF.

REFERENCES

- [1] Petrovic, V. et al. Additive layered manufacturing: sectors of industrial application shown through case studies. *Int. J. Prod. Res.* 49, 1061–1079 (2011).
- [2] Buchbinder, D., Schleifenbaum, H., Heidrich, S., Meiners, W. & Bültmann, J. High Power Selective Laser Melting (HP SLM) of Aluminum Parts. *Phys. Procedia* 12, 271–278 (2011).
- [3] Aboulkhair, N. T., Everitt, N. M., Ashcroft, I. & Tuck, C. Reducing porosity in AlSi10Mg parts processed by selective laser melting. *Addit. Manuf.* 1–4, 77–86 (2014).
- [4] Thijs, L., Verhaeghe, F., Craeghs, T., Humbeeck, J. Van & Kruth, J.-P. A study of the microstructural evolution during selective laser melting of Ti-6Al-4V. *Acta Mater.* 58, 3303–3312 (2010).
- [5] Weingarten, C. et al. Formation and reduction of hydrogen porosity during selective laser melting of AlSi10Mg. *J. Mater. Process. Technol.* 221, 112–120 (2015).
- [6] Gibson, I., Rosen, D. & Stucker, B. *Additive Manufacturing Technologies*. (Springer New York, 2015). doi:10.1007/978-1-4939-2113-3.
- [7] Kruth, J. P., Wang, X., Laoui, T. & Froyen, L. Lasers and materials in selective laser sintering. *Assem. Autom.* 23, 357–371 (2003).
- [8] Zhang, D. et al. Metal Alloys for Fusion-Based Additive Manufacturing. *Adv. Eng. Mater.* 20, 1700952 (2018).
- [9] Gong, H. et al. Influence of defects on mechanical properties of Ti-6Al-4V components produced by selective laser melting and electron beam melting. *Mater. Des.* 86, 545–554 (2015).
- [10] Malekipour, E. & El-Mounayri, H. Common defects and contributing parameters in powder bed fusion AM process and their classification for online monitoring and control: a review. *Int. J. Adv. Manuf. Technol.* 95, 527–550 (2018).
- [11] Khairallah, S. A., Anderson, A. T., Rubenchik, A. & King, W. E. Laser powder-bed fusion additive manufacturing: Physics of complex melt flow and formation mechanisms of pores, spatter, and denudation zones. *Acta Mater.* 108, 36–45 (2016).
- [12] Badiru, A. B., Valencia, V. V & Liu, D. *Additive Manufacturing Handbook: Product Development for the Defense Industry*. (CRC Press, 2017).
- [13] King, W. E. et al. Observation of keyhole-mode laser melting in laser powder-bed fusion additive manufacturing. *J. Mater. Process. Technol.* 214, 2915–2925 (2014).
- [14] Shrestha, S., Starr, T. & Chou, K. Porosity Analysis in Metal Additive Manufacturing by Micro-CT. in *Volume 2: Advanced Manufacturing* (American Society of Mechanical Engineers, 2018). doi:10.1115/IMECE2018-87897.
- [15] Choo, H. et al. Effect of laser power on defect, texture, and microstructure of a laser powder bed fusion processed 316L stainless steel. *Mater. Des.* 164, 107534 (2019).
- [16] Åsberg, M., Fredriksson, G., Hatami, S., Fredriksson, W. & Krakhmalev, P. Influence of post treatment on microstructure, porosity and mechanical properties of additive manufactured H13 tool steel. *Mater. Sci. Eng. A* 742, 584–589 (2019).
- [17] Morrow, B. M. et al. Impact of Defects in Powder Feedstock Materials on Microstructure of 304L and 316L Stainless Steel Produced by Additive Manufacturing. *Metall. Mater. Trans. A* 49, 3637–3650 (2018).
- [18] Gu, D. et al. Densification behavior, microstructure evolution, and wear performance of selective laser melting processed commercially pure titanium. *Acta Mater.* 60, 3849–3860 (2012).
- [19] Cunningham, R. et al. Analyzing the effects of powder and post-processing on porosity and properties of electron beam melted Ti-6Al-4V. *Mater. Res. Lett.* 5, 516–525 (2017).
- [20] Qiu, C. et al. Influence of processing conditions on strut structure and compressive properties of cellular lattice structures fabricated by selective laser melting. *Mater. Sci. Eng. A* 628, 188–197 (2015).
- [21] Thijs, L., Kempen, K., Kruth, J.-P. & Van Humbeeck, J. Fine-structured aluminium products with controllable texture by selective laser melting of pre-alloyed AlSi10Mg powder. *Acta Mater.* 61, 1809–1819 (2013).
- [22] Yang, K. V. et al. Porosity formation mechanisms and fatigue response in Al-Si-Mg alloys made by selective laser melting. *Mater. Sci. Eng. A* 712, 166–174 (2018).
- [23] Yang, K. V., Rometsch, P., Davies, C. H. J., Huang, A. & Wu, X. Effect of heat treatment on the microstructure and anisotropy in mechanical properties of A357 alloy produced by selective laser melting. *Mater. Des.* 154, 275–290 (2018).
- [24] Tang, M. & Pistorius, P. C. Oxides, porosity and fatigue performance of AlSi10Mg parts produced by selective laser melting. *Int. J. Fatigue* 94, 192–201 (2017).
- [25] Das, S. *Physical Aspects of Process Control in Selective Laser Sintering of Metals*. *Adv. Eng. Mater.* 5, 701–711 (2003).
- [26] Romano, S., Beretta, S., Brandão, A., Gumpinger, J. & Ghidini, T. HCF resistance of AlSi10Mg produced by SLM in relation to the presence of defects. *Procedia Struct. Integr.* 7, 101–108 (2017).
- [27] Sheridan, L., Scott-Emuakpor, O. E., George, T. & Gockel, J. E. Relating porosity to fatigue failure in additively manufactured alloy 718. *Mater. Sci. Eng. A* 727, 170–176 (2018).

- [28] Prithvirajan, V. & Sangid, M. D. The role of defects and critical pore size analysis in the fatigue response of additively manufactured IN718 via crystal plasticity. *Mater. Des.* 150, 139–153 (2018).
- [29] Grasso, M. & Colosimo, B. M. Process defects and in situ monitoring methods in metal powder bed fusion: a review. *Meas. Sci. Technol.* 28, 044005 (2017).
- [30] Bauereiß, A., Scharowsky, T. & Körner, C. Defect generation and propagation mechanism during additive manufacturing by selective beam melting. *J. Mater. Process. Technol.* 214, 2522–2528 (2014).
- [31] Wang, P. et al. Scanning optical microscopy for porosity quantification of additively manufactured components. *Addit. Manuf.* 21, 350–358 (2018).
- [32] Kim, F. H., Moylan, S. P., Garboczi, E. J. & Slotwinski, J. A. Investigation of pore structure in cobalt chrome additively manufactured parts using X-ray computed tomography and three-dimensional image analysis. *Addit. Manuf.* 17, 23–38 (2017).
- [33] Maskery, I. et al. Quantification and characterization of porosity in selectively laser melted Al–Si10–Mg using X-ray computed tomography. *Mater. Charact.* 111, 193–204 (2016).
- [34] Slotwinski, J. A., Garboczi, E. J. & Hebenstreit, K. M. Porosity Measurements and Analysis for Metal Additive Manufacturing Process Control. *J. Res. Natl. Inst. Stand. Technol.* 119, 494 (2014).
- [35] Zhang, B., Li, Y. & Bai, Q. Defect Formation Mechanisms in Selective Laser Melting: A Review. *Chinese J. Mech. Eng.* 30, 515–527 (2017).
- [36] Ferrar, B., Mullen, L., Jones, E., Stamp, R. & Sutcliffe, C. J. Gas flow effects on selective laser melting (SLM) manufacturing performance. *J. Mater. Process. Technol.* 212, 355–364 (2012).
- [37] Nazari, K. A., Nouri, A. & Hilditch, T. Compressibility of a Ti-based alloy with varying amounts of surfactant prepared by high-energy ball milling. *Powder Technol.* 279, 33–41 (2015).
- [38] Leung, C. L. A. et al. The effect of powder oxidation on defect formation in laser additive manufacturing. *Acta Mater.* 166, 294–305 (2019).
- [39] Milewski, J. O. *Additive Manufacturing of Metals: From Fundamental Technology to Rocket Nozzles, Medical Implants, and Custom Jewelry.* (Springer International Publishing, 2017).
- [40] Gong, H., Rafi, K., Gu, H., Starr, T. & Stucker, B. Analysis of defect generation in Ti–6Al–4V parts made using powder bed fusion additive manufacturing processes. *Addit. Manuf.* 1–4, 87–98 (2014).
- [41] Iebba, M. et al. Influence of Powder Characteristics on Formation of Porosity in Additive Manufacturing of Ti–6Al–4V Components. *J. Mater. Eng. Perform.* 26, 4138–4147 (2017).
- [42] Tong, J., Bowen, C. R., Persson, J. & Plummer, A. Mechanical properties of titanium-based Ti–6Al–4V alloys manufactured by powder bed additive manufacture. *Mater. Sci. Technol.* 33, 138–148 (2017).
- [43] Seifi, M., Salem, A., Satko, D., Shaffer, J. & Lewandowski, J. J. Defect distribution and microstructure heterogeneity effects on fracture resistance and fatigue behavior of EBM Ti–6Al–4V. *Int. J. Fatigue* 94, 263–287 (2017).
- [44] Mower, T. M. & Long, M. J. Mechanical behavior of additive manufactured, powder-bed laser-fused materials. *Mater. Sci. Eng. A* 651, 198–213 (2016).
- [45] Körner, C., Bauereiß, A. & Attar, E. Fundamental consolidation mechanisms during selective beam melting of powders. *Model. Simul. Mater. Sci. Eng.* 21, 085011 (2013).
- [46] Sola, A. & Nouri, A. Microstructural porosity in additive manufacturing: The formation and detection of pores in metal parts fabricated by powder bed fusion. *J. Adv. Manuf. Process.* 1, (2019).

02 Metal Additive Manufacturing: Design Keys

E. Toyserkani, D. Sarker, O.O. Ibhadode, *et al.*

MATERIALS: STRUCTURE-PROPERTY RELATIONSHIP

In materials science, besides the structure and property of materials, two other major components are processing and performance since the processing route will determine the final material structure.

Material properties are correlated with the microstructure, which can be modified by changing the micro constituents' relative magnitude, known as phases. In the microstructure, phases are categorized according to their distinctive crystal structures, elemental composition, and properties. These properties affect the performance of materials in applications and alter their performance. The modification of microstructure can be done by adding new elements or processing through mechanical and thermal treatments.

Thermomechanical treatments (a combination of mechanical and thermal treatments) are used to yield properties that cannot be achieved using other techniques. Hot isostatic pressing (HIP), which exposes manufactured parts to simultaneously elevated temperature and isostatic gas pressure in a high-pressure containment vessel, may also be used to minimize porosity while changing the phases.

MANUFACTURING OF METALLIC MATERIALS

Distinct from traditional fabrication methods, additive manufacturing (AM) is a technique of producing three-dimensional solid products of any geometry using a digital model. It follows an additive method, where materials are added in consecutive layers and are differentiated from conventional subtractive machining techniques based on the subtraction of materials through cutting or milling.

The manufacture of AM metal powder comprises three stages:^[1]

- i. Mining and extracting ore to fabricate pure metal or alloy products
- ii. Powder production
- iii. Powder sorting, classification, and validation

The powder morphology has a substantial effect on bulk packing and flow behaviors. Spherical, regular, and equiaxed powders can organize and pack more competently than irregular powders. However, reports are claiming that irregular powders behave well in terms of flowability in the AM powder bed and powder-fed processes for many applications. The powder morphology can significantly influence the density of final AM components. Very spherical powders are more advantageous to AM processes. On the other hand, this, in fact, reduces the use of possibly cheaper powder manufacturing methods. Recent research outcomes demonstrate that the more irregular the powder shape, the inferior the product density.^[2] Powder size distribution is another vital parameter, and it can impact the size of layer thickness and the finest aspect of the AM products.

SOLIDIFICATION IN ADDITIVE MANUFACTURING: NON-EQUILIBRIUM

The laser- or electron-beam (EB)-based AM methods entail a localized moving heat source with a very short interaction time. As the point heat source delivers extremely focused energy, it causes vastly localized heat flux in the melt pool zone, together with a massive temperature gradient in the deposited layers. The temperature gradient at the bottom of the substrate surface is higher compared to the top of the deposited surface. During the solidification process, the alloy partition coefficient drops, which results in the rejection of solute atoms at the solid-liquid boundary. The concentration of solute atoms rises until the solution reaches a steady condition. The solidification temperature at the solid-liquid boundary is influenced by the liquid composition, as well as

the processing speed and angle of this boundary with respect to the heat source centerline.

AM is comparatively a rapid solidification process.^[3] There are two main reasons for rapid solidification: (i) enormous undercooling of the melt and (ii) fast-moving temperature fluxes.^[4] A common feature of rapid solidification is accompanied by robust liquid flow, such as Marangoni convection, where flow velocities can be as high as 1–4 m/s. In the rapid solidification mode, elemental partitioning is reduced, which extends the solid solubility that may cause the formation of metastable phases. In addition, because of the directional heat conduction, a preferred directionality in grain growth may occur. The combined influence of rapid and directional solidification and phase transformation persuaded by continual thermal cycles has a substantial influence on the deposited parts' microstructure.

Rapid solidification characteristics can be summarized as the refinement of microstructure, an increase of solubility limits, lessening of micro segregation, and non-equilibrium of metastable phase formation.^[10] The formation of distinctive microstructural features such as grains, lamellae, and second-phase particles is generally reduced in the fast cooling compared to the standard casting methods.^[5] Another possible outcome is the mitigation of dendritic segregation at a point where compositional homogeneity can be attained.^[5]

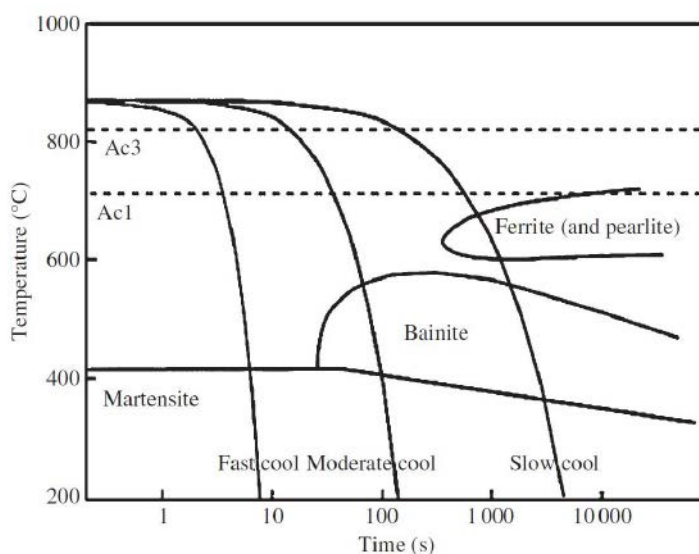


Figure 1: Continuous cooling transformation diagram for steel.
[Source: Openly accessible through creative commons license.]

EQUILIBRIUM SOLIDIFICATION

The structure of a material, which is a function of composition and temperature, can be identified from an equilibrium phase diagram using the assumption of a relatively slow transformation rate or a faster diffusion rate.

Cooling Curve and Phase Diagram

A cooling curve is a graphical presentation of the phase transition temperature with time for pure metals or alloys over a complete temperature range. On the other hand, a phase diagram is a useful tool to understand the formation of phases and their transformation throughout the heating and cooling practice with different alloy compositions. For example, during the manufacturing of stainless steel using laser-based AM technology, it is crucial to optimize the laser input temperature to control the austenite and ferrite phase formation.

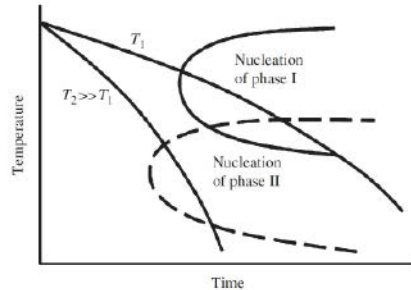
Another important tool is the continuous cooling transformation (CCT) diagram, which presents the knowledge of the type of phases that will form in alloys at different cooling rates. It is vital in AM techniques since each deposited layer goes through repeated thermal cycles and eventually has different cooling rates. A CCT diagram for steel is shown in **Figure 1**, where it is evident that a complete martensitic structure forms at fast cooling conditions, whereas bainite, ferrite, and pearlite can occur at relatively slower cooling rates. In the AM process, when the thermal profile of each deposited layer is known, the CCT diagram can be used to estimate the formation of phase types.

NON-EQUILIBRIUM SOLIDIFICATION

The most significant part of the solidification of AM is the heating and cooling cycle, which may cause suppressed phase changes or supersaturated phases. In AM, when every layer passes through a repeated heating and cooling cycle, the temperature in the layer may reach above the phase transformation temperature. This will result in the multiple phase transformation or intricate microstructure, in addition to a residual stress formation.

For better control of microstructure in AM parts, knowledge of the phase transformation during the fast solidification and repeated thermal cycle behaviors is essential. During the rapid cooling, some phases that generally form under equilibrium conditions may not

Figure 2: Time-temperature diagram presenting the nucleation onset of two dissimilar theoretical phases with different cooling behaviors.



arise; hence, there would be a chance for the occurrence of metastable phases. The characteristics of the metastable phases are based on the alloy chemical structure and thermal behavior of the cooling method. This aspect is graphically emphasized in **Figure 2**. From the time-temperature diagram, at cooling rate T_1 , the primary phase is nucleated as phase I, whenever at a faster cooling rate T_2 , ($T_2 \gg T_1$); another phase, phase II is nucleated by detouring phase I. To clarify the phase formation, a phase diagram is shown in **Figure 3**, where phase δ is evident at equilibrium conditions. Due to the rapid cooling process, a metastable phase diagram may be created, which is highlighted by the dashed lines. In this cooling condition, if the delta phase cannot generate, a eutectic system may appear at a lower temperature with different chemical compositions compared to the equilibrium phase diagram.

SOLUTE REDISTRIBUTION AND MICRO SEGREGATION

Micro segregation is defined as the ejection of solute from the freezing material, which afterward distributes heterogeneously and eventually affects the solidification mode. The alloy in liquid form contains a higher solute compared to the solidified condi-

tion. Therefore, during the solidification process, there is a chance of the high solute liquid being trapped within the solidified structures. This causes micro segregation or banding of high and low solute alloys and substantial incoherence in material properties.^[10]

The theory and mechanism of solute redistribution can be expressed using equilibrium and non-equilibrium models, considered in the vigorous conditions of solute redistribution. The factors that are assumed in equilibrium lever laws are (i) complete diffusion in both liquid and solid-state (ii) equilibrium at solid/liquid boundary, and (iii) no undercooling through the growth. Additionally, in the non-equilibrium lever law (Scheil equation), similar assumptions are considered, apart from considering negligible diffusion in the solid. In solidification, these three factors signify the extreme situations of residual micro segregation. According to the equilibrium lever law, there are no concentration gradients in the liquid and solid during solidification and eventually no residual micro segregation in the solidified structure. On the other hand, the non-equilibrium situation possesses residual micro segregation in the solidified structure because of very minor solid diffusivity.

Generally, the solute diffusion coefficient of a solid phase is about four times lower than a liquid phase; therefore, a precise image of plane front solidification is expressed by a hypothesis that no diffusion happens in the solid phase and complete mixing of liquid occurs. However, as the solute is not endorsed to mix in the solid phase, an uneven concentration profile grows behind the progressing interface. The liquid concentration remains consistent with the hypothesis of thorough mixing. An equilibrium solute concentration at the developing solid-liquid interface may be of interest to develop an expression for the shape of the solute concentration in a solid.

Three different categories of solute redistribution are presented in **Figure 4**, which can form with insignificant diffusion in the solid. For type 1, the liquid diffusion or convection-controlled mixing in the liquid is finished or the subsequent solute segregation is vigorous. In contrast, for type 3, liquid diffusion is incomplete without convection-controlled mixing in the liquid and, eventually, the solute segregation is less vigorous. However, type 2 shows intermediate behavior to types 1 and 3, which ensure solute segregation^[10]. Therefore, based on the relations between the alloying elements, there

Figure 3: A comparative presentation of the theoretical equilibrium (solid lines) and metastable non-equilibrium phase diagram (dotted lines).

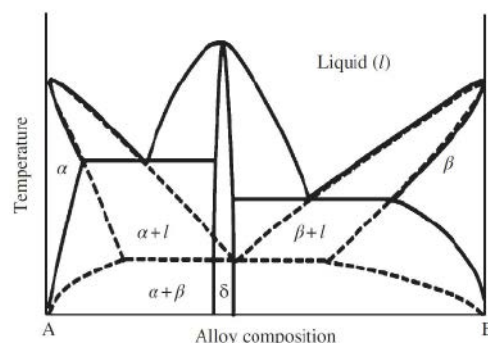
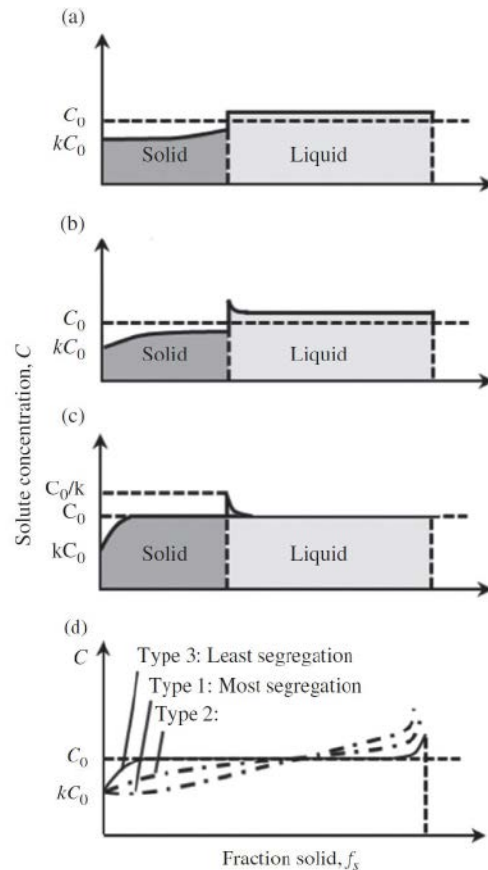


Figure 4: Solute distribution without diffusion in the solid and dissimilar diffusion in the liquid. (a) Type 1: complete liquid diffusion or mixing, (b) Type 2: limited liquid diffusion, some convection, (c) Type 3: limited liquid diffusion, no convection, (d) combination of Type 1, 2, and 3.^[10]
 [Source: Reproduced with permission from John Wiley & Sons Inc.]



will be remarkable importance on the diffusion rates, temperature, and various concentration profiles at the boundary during solidification.

CONSTITUTIONAL SUPER-COOLING

Usually, in the solidification process, the material in the liquid form first cools at the phase transformation temperature and then starts to solidify with the release of its latent heat.^[7] As the cooling progresses, the temperature of the liquid continues to drop. However, the system becomes thermodynamically unstable. Therefore, solidification can be commenced with a small amount of energy accomplished with the latent heat release, which eventually increases the temperature. The real temperature at which the solidification starts is termed "the degree of supercooling." This occurs because of the alloying element segregation at the solid-liquid boundary.^[8] The additional concentration of the elements lowers the melting temperature of the liquid. When this reduction is adequate to drop the melting temperature far below the actual temperature, then the liquid will be locally supercooled.

Constitutional supercooling considers the interactions between the temperature gradient, interface speed, and the alloying element to develop a simple criterion to forecast the position of the melt, whether it is above or below the liquid. In the former position, the melt remains steady to a lump on the interface that advances shortly into the melt. In the latter position, the melt is supercooled to solidify naturally on any interface lump.^[9]

NUCLEATION AND GROWTH KINETICS

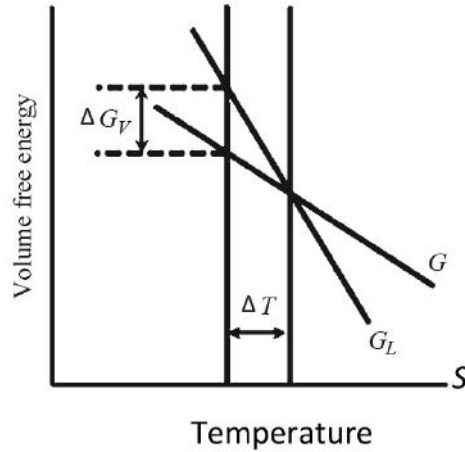
In the rapid solidification of a supercooled alloy, the nucleation mechanism is far different from the conventional one. For the highly supercooled pure metals and solid solution alloys, a single nucleation event may be adequate to start and complete the solidification process having a faster crystal growth rate. But the growth of the supercooled material is always diffusion-controlled, which inherently entails a sluggish growth behavior. Therefore, the question is whether a single nucleation matter can lead to the solidification system.

Generally, in most AM techniques, the deposited material in every layer has a similar chemical composition unless a powder-fed directed energy deposition is utilized, in which the powder stream may change from one composition to others on demand. In these circumstances, due to a similar crystal structure, epitaxial growth can eliminate nucleation and let the natural growth happen without activation energy until below the liquidus temperature. On the other hand, when dissimilar materials are deposited during the fabrication of composites, or surface cladding of AM, then the nucleation phenomenon should be considered. In layer-by-layer AM processes, this may also happen when the first layer is deposited on the dissimilar substrate material. When nucleation occurs at the solid/liquid boundary, the newly formed phase needs to conquer an energy obstacle that eventually controls the structure and property of the solidified part.

Nucleation

Nucleation is classified into (i) homogeneous nucleation and (ii) heterogeneous nucleation. Homogeneous nucleation occurs with the formation of uniform nuclei all over the parent phase, while in heterogeneous nucleation, nuclei may advance from the structural discontinuity, such as boundaries of the impurities, foreign particles, dislocations, and so on.

Figure 5: Schematic presentation on the relation between the Gibbs free energy and undercooling temperature.



Considering a relation between the Gibbs free energy and the undercooling temperature shown in **Figure 5**, when a liquid cools far below its melting point (T_m), the Gibbs free energy (G_S) for the solid becomes lower than the liquid (G_L). There would be an undercooling temperature ΔT and a driving force ΔG to result in an impulsive phase transformation.^[12] The volume of free energy can be expressed as:

$$\Delta G_V = G_L - G_S \quad \text{Eq. 1}$$

Briefly, the solidification of pure metal is considered in **Figure 6**, where nuclei of a solid phase (spherical, with a radius r) are formed inside of a liquid-like packing arrangement of clustered atoms.^[13] In addition, **Figure 6b** presents two energy sources for the total free

energy evolution that conduct a solidification transformation. The first source is the difference between free energy within the solid and liquid, known as the volume free energy, ΔG_V . It becomes negative when the temperature drops down the equilibrium, where it is quantified by the product of nucleus volume (i.e., $4\pi r^3/3$). The second energy source comes from the development of a solid/liquid interface through the solidification process. This is a surface-free energy γ with a positive value, which is quantified by the product of the nucleus surface area (i.e., $4\pi r^2$). Therefore, the complete energy change ΔG is the addition of those two energy sources,

$$\Delta G = -\frac{4}{3} \pi r^3 \Delta G_V + 4\pi r^2 \gamma_{sl} \quad \text{Eq. 2}$$

From a physics point of view, when solid particles in the liquid cluster together to form atoms, their free energy rises. After reaching the size of a critical radius r^* , the growth of the clustered atoms begins with a decline of free energy. In contrast, below the critical size, the cluster will shrink or dissolve. This critical size particle is known as an *embryo*, whereas with greater size, it is called a nucleus. The free energy that arises at the critical radius is the critical free energy ΔG^* , which is the highest of the curve in **Figure 6b**. This is actually an activation of free energy required to form a stable nucleus, or equally as an energy barrier in the nucleation process.

The criterion to begin a nucleation process can be theoretically derived from the condition $d(\Delta G)/dr=0$, and $r^* = 2\gamma_{sl}/\Delta G_V$.

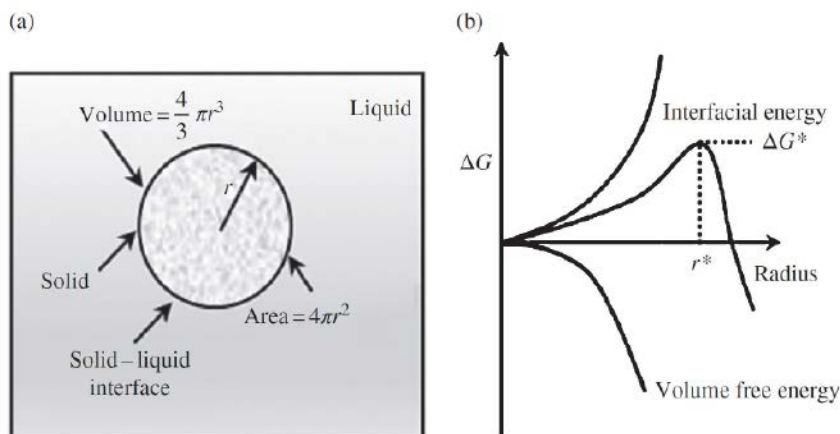


Figure 6: (a) A figure depicting the nucleation of a sphere-shaped particle in a liquid. (b) A plot of free energy against embryo/nucleus radius, where it also presented the critical free energy change (ΔG_V) and the critical nucleus radius (r^*).^[13]
[Source: Reproduced with permission from John Wiley and Sons.]

In heterogeneous nucleation or epitaxial growth, a nucleus in a liquid is formed in connection with a substrate. Therefore, the interfacial energies between the liquid, nucleus solid, and substrate metal control the geometry of the nucleus.^[14] The total energy can be reduced by assuming the nucleus as the geometry of a spherical cap, as presented in **Figure 7a**. At equilibrium, the interfacial energy is equal to $\gamma_{ML} = \gamma_{SM} + \gamma_{SL} \cos \varnothing$, where γ_{ML} represents the interfacial energy between the substrate and the liquid, γ_{SM} is the interfacial energy within the solid nucleus and substrate, and γ_{SL} is the interfacial energy between the solid nucleus and liquid. In addition, \varnothing is the contact angle of the nucleus. When the chemical composition of the substrate and the nucleus are identical, then the interfacial energy between them is negligible. Moreover, the interfacial energies between the substrate and liquid are similar to the interfacial

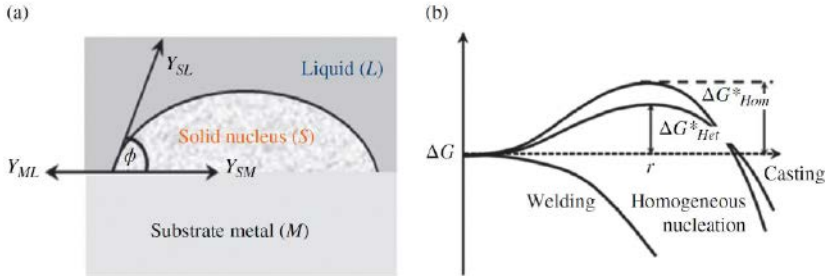


Figure 7: (a) Solid nucleus connected with substrate metal and liquid. (b) Graphic presentation for free energy change related to heterogeneous nucleation observed in casting and welding together with homogeneous nucleation.^[14]

[Source: reproduced with permission from John Wiley and Sons.]

energies between the nucleus and liquid. The free energy change related to the creation of a solid spherical cap of radius r is shown by:

$$\Delta G_{\text{het}} = -V_S \Delta G_V + A_S \gamma_{SL} \quad \text{Eq. 3}$$

$$\Delta G_{\text{het}} = S(\varnothing) \left[-\frac{4}{3} \pi r^3 \Delta G_V + 4\pi r^2 \gamma_{SL} \right] \quad \text{Eq. 4}$$

where ΔG_V is the free energy change per unit volume, accompanying the nucleus development, V_S is the volume of the nucleus, A_S is the surface area of the interface between the nucleus and the liquid, and $S(\varnothing)$ is the shape factor, which depends on the contact angle. By adopting differentiation of the above equation for r , and considering the result as zero, the critical radius of the heterogeneous nucleation is presented as $r_{\text{het}}^* = 2\gamma_{SL} / \Delta G_V$. The energy obstruction for the heterogeneous nucleation is then:

$$\Delta G_{\text{het}} = \frac{16\pi\gamma_{SL}^3}{3\Delta G_V^2} S(\varnothing) \quad \text{Eq. 5}$$

In epitaxial solidification, \varnothing is zero and so $S(\varnothing)$ approaches zero, which makes ΔG_{het} zero as well. It emphasized that the energy barrier for the epitaxial solidification is negligible contrasted to the casting or other processes, as shown in **Figure 7b**. Because of this small energy barrier, the initiation of nucleation is very fast in epitaxial solidification. Usually, in metal AM, the chemical composition of the solid and liquid is pretty similar, which makes γ_{SL} small, as well as the critical radius. On the other hand, this type of solidification demands incomplete or through melt-back of the substrate to expedite grain evolution from the existing ones. The melt-back of the earlier solidified layer is critical in the context of the continuity of the microstructure through the successively melted and solidified multiple layers.

Growth Behavior

After the initiation of the nucleation, the solid/liquid interface deems as a growth front. The growth kinetics is dominated by the roughness of the solid/liquid interface on the atomic scale, which may be atomically rough (in metals) or atomically flat (in non-metals). The first one progresses with continuous growth, whereas the second one follows lateral growth, including nucleation and dispersion of ledges.^[15]

Growth starts from the previously deposited layers through partial or complete melting, which eventually governs the crystallographic pattern.^[11,16] The intensified heat may penetrate further below the deposited layers, enabling the remelting process required to eliminate surface contaminants and the breakdown of oxides, thus offering a clean solid/liquid interface. The microstructure developed close to the melt boundary is controlled by the substrate material, whereas far away from the boundary, it is advanced through competitive growth.^[17]

Usually, competitive growth takes place between dendrites with numerous crystallographic orientations and is commonly found in alloys of iron,^[18,19] nickel,^[20] titanium,^[21] and tantalum.^[22] Dendrites normally progress by the path of higher heat flow and lead to competitive growth in the structure.

When the solute-rich boundary layer creates a temperature gradient sharper than a critical gradient for constitutional supercooling, a stable planar interface growth is introduced.^[15] If constitutional supercooling is encountered, successive lumps at the solidification front may propagate with rapid growth to advance into long arms or cells, approaching parallel to the heat flow and developing a cellular microstructure. However, with a smaller temperature gradient, a broader "mushy zone" is formed, which advances dendritic growth with secondary or tertiary arms.

Combined, the base metal at the boundary line plays as a nucleation site.^[10] As the liquid metal within the melt pool is closely touching the thin layer of a substrate while completely splashing them, nucleation progresses without difficulties. During the autogenous joining, nucleation starts with the agglomeration of atoms in the liquid on the previously developed structures continuing with similar crystallographic orientations. This type of growth phenomenon is shown in **Figure 8** and is known as epitaxial nucleation or epitaxial growth. The

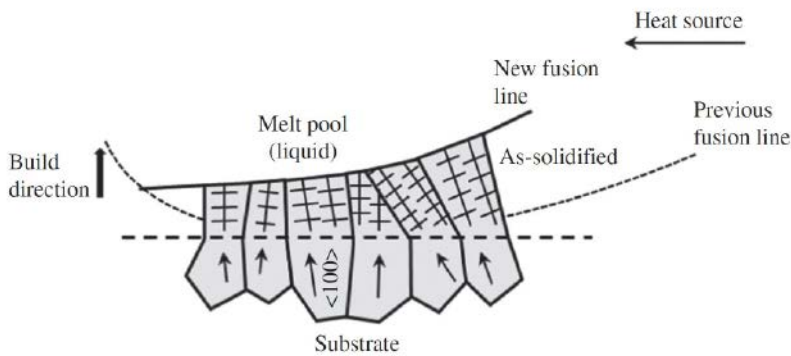


Figure 8: Epitaxial growth of the solidified metal adjacent to the fusion line.^[10]
 [Source: Reproduced with permission from John Wiley & Sons Inc.]

figure describes the grains' growth with 100 crystallographic orientations, which is common for the face-centered-cubic or body-centered-cubic crystal structures, where columnar grains advance in the 100 direction.

SOLIDIFICATION MICRO-STRUCTURE IN PURE METALS AND ALLOYS

The solidification process may be stable or unstable. Stable solidification is defined as a smoothly growing interface, responsible for the thermal diffusion through the solid phase. In these circumstances, the surface tension and the dynamic movement at the interface are neglected, thus with reduced perturbation. However, unstable solidification occurs when the metastable liquid cools far below the equilibrium temperature. In this situation, thermal diffusion from the interface occurs both in solid and liquid phases when the surface tension and dynamic movement are also considered. The local perturbation on the boundary layer will be enriched, and further protrusion in the liquid will progress with various structural patterns. The formation of

grain pattern and the crystallographic texture is controlled by the melting process and the solidification of the liquid melt zone.

The melt area drives away heat through the substrate causing the melt pool to have a curved shape. Depending on the process parameters, the melt pool shape may vary from oval or tear-drop-shaped on the substrate with a semicircular or keyhole cross-section. The geometric profile of the melt pool is significant as it affects the grain structure in the fusion zone. In the keyhole case, the beam goes down the substrate with minimum heat input, which changes the conduction mode at high speeds equally in electron and laser beam techniques. The conduction approach is desired for AM because of the unsteady keyhole that may cause undesired porosity in AM products.

There are four major solidification patterns: (i) planar, (ii) cellular, (iii) columnar, and (iv) equiaxed dendritic (**Figure 9**). The various solidification structures grow depending on the driving force of constitutional supercooling, the distribution of the solute at the boundary, as well as the characteristics of the elements contained in the solidified alloys. Generally, the devastating forces of constitutional supercooling do not exist in pure metal, which will then show a planar solidification approach.^[10]

The relation between the different solidification patterns with the degree of constitutional supercooling is shown in **Figure 10**. A planar solidification starts with a greater real temperature in contrast to the equilibrium temperature of the liquid melt.^[23] In the planar solidification, a stochastic protuberance may grow into an area of higher temperature and results in the breakdown of the protuberance (**Figure 10a**). Planar solidification is feasible, especially for single crystal growth, where it demands either high purity metal or tremendously high degrees of temperature gradients or solidification rate.

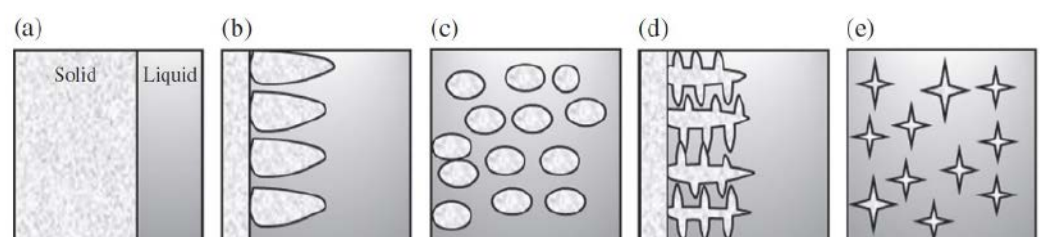


Figure 9: The schematic diagrams illustrate the modes of solidification pattern: (a) planar, (b) and (c) cellular, (d) columnar dendritic, and (e) equiaxed dendritic.

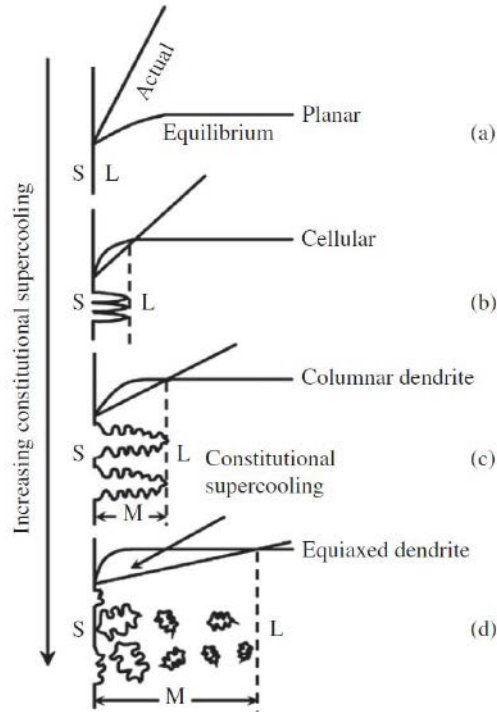


Figure 10: Occurrence of various solidification structures related to constitutional supercooling.^[10]

[Source: Reproduced with permission from John Wiley & Sons Inc.]

In constitutional supercooling, the real temperature gradient is lower than the liquid's temperature gradient; a protuberance may mature in the undercooled melt and approach as a cellular or dendritic pattern (**Figure 10b**). When the grain grows like a column without branching the arms, it will form a cellular structure. In contrast, the grains with secondary or tertiary arms will develop a dendritic structure (**Figures 10c and 10d**). The cellular and dendritic growth are estimated by the degree of constitutional supercooling and the complete stability described by the critical solidi-

fication rate. However, planar solidification is independent of the temperature gradient.

Generally, the solidification starts homogeneously after adequate cooling or heterogeneously with the existence of a solid particle in the supercooled melt. Moreover, after nucleation, the consequent growth of the solid from the particle may be unstable, and based on the degree of supercooling, dendritic structures start to form. Dendrites are defined as prototypical structures growing from homogeneous initial states into compound spatio-temporal configurations distinct from equilibrium.

The root of the word "dendrite" originates from the Greek term "dendron," meaning "tree". Similar to a tree, a dendrite shows an extremely branched, arborescent pattern, which is schematically presented in **Figure 11**.

Because of the unsteadiness of the interface, a dendrite structure comprises the primary stem, secondary, or tertiary branches, all advancing in particular crystallographic directions. The dendritic structures in metallurgy form the microstructure of metals or alloys, which heavily controls the mechanical, chemical, and physical characteristics of the material. During the solidification, the growth of the perturbation at the solid/liquid boundary may be inhibited by the surface tension or kinetic phenomenon. The challenge between the steady influence of surface tension and the unsteady influence of supercooling is mainly the cause source for the formation of dendritic compound patterns.

As the grain structure influences the mechanical properties, it is essential to create finer grains in the solidified material to achieve superior properties. However, in laser or EB metal AM, it is crucial to stop grain growth during remelting of the formerly deposited layers, which also brings heterogeneous nucleation and epitaxial grain development either in cellular or dendritic form. When the epitaxial grain growth of the columnar grains is prevented by the development of equiaxed grains close to the melt zone area, and the equiaxed grains are deeper than the remelted penetration depth, then the equiaxed grains govern the average grain size. It is demanded in laser or EB-based AM that the occurrence of equiaxed grains is estimated by the density of heterogeneous nucleation sites, which may be feasible in the laser powder bed fusion (LPBF) process with a proper powder feed rate.

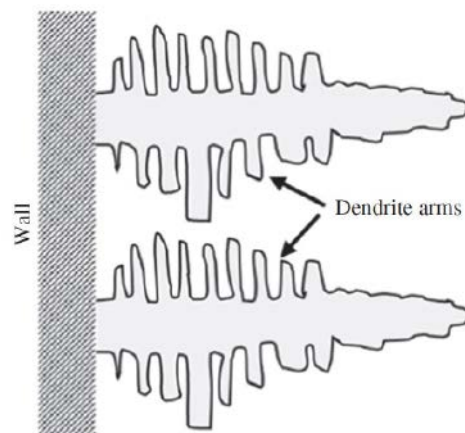


Figure 11: Schematic of the dendrite formation/growth.

DIRECTIONAL SOLIDIFICATION IN AM

The most vital factor in controlling the mechanical properties of AM products is the solidification structure.^[6] The connection with higher laser energy provides rapid heating and cooling, resulting in faster solidification during cooling. Moreover, the heat dissipation rate through the substrate is fast enough to develop a rapidly solidified structure. Therefore, grain refinement is usually predicted in the distinctive AM structures because of their inadequate time for grain formation/progression.

The solute intensity or temperature gradients in the melt may produce surface tensions and subsequent Marangoni convection, resulting in an unstable solidification process. Moreover, rapid solidification generally progresses along with the maximum heat flow. The mechanisms of non-equilibrium solidification and the propensity for directional propagation are instantaneous but competitive, which may generate diversity in crystal orientation with limited consistency. As a result, AM-processed metallic products may possess intrinsic anisotropic characteristics.

For a known material composition, the solidification morphology is controlled by parameters such as solidification velocity and temperature gradient. The developed structure may differ from planar to cellular and to dendrites, which normally turn into a finer structure until the regeneration of cellular structures with a growth rate of near-absolute stability. At velocities greater than this range, the banding acts, and finally, the planar interface is completely stabilized. The well-developed cellular structure normally grows without advancing side arms, where their axes are aligned to the heat flux direction without considering any crystal orientation. However, dendrites are regarded as the growth of their arms along crystallographic orientations. Because of the anisotropy in solid/liquid interface energy and growth mechanism, cubic crystal dendrite will propagate along the 001 direction, indicating the heat flow direction.

Throughout the directional solidification and advance of columnar structures, the heat flux follows contrary to the growth direction. This means that the growth rate of the fronts limits the solid/liquid boundary to propagate at this rate. During the alloy solidification, the solute will stack on the boundary, while the distribution coefficient is normally lower than the

unity and, eventually, this variation of concentration will impact the equilibrium solidification temperature. The supercooled zone, where equiaxed grains with various volume fractions may take place, depends on the thermal gradient and the solidification rate, and finally directs to the columnar-to-equiaxed transition.

FACTORS AFFECTING SOLIDIFICATION IN AM

Cooling Rate

Generally, solidification/cooling rates are influenced by the heat input, which is manipulated by the laser or EB power, beam scan speed layer thickness, scanning strategies, etc. When the laser power is low and scanning speed is high, this combination normally delivers a smaller heat flux that results in a larger cooling rate. In contrast, with higher laser power and lower scan speed, heat input would be intensified to melt a larger substrate area, which eventually results in a slower cooling rate.

Temperature Gradient and Solidification Rate

Through solidification, columnar grains advance along the path of a higher temperature gradient in the melt pool.^[16] The spherical melt pool generates curved and tapered columnar structures because of the deviation in the thermal gradient path from the pool border. However, the comet-featured melt pool creates conventional and wide columnar structures, where the path of the maximum thermal gradient does not shift notably through the process.

If we consider the angle between the direction of grain growth and beam scan speed (SS) is θ , then the constant nominal growth rate R_N would be $R_N = SS \cdot \cos\theta$. In a cubic crystal structure, the $\langle 100 \rangle$ direction designates the main dendrite growth direction. This favored growth direction makes the local growth rate R_L greater than the nominal rate R_N . Another angle ϕ is considered between the normal direction of the melt pool border and the $\langle 100 \rangle$ direction to link R_L and R_N , which is $R_L = R_N / \cos\phi$. The relationship states that the local growth rate becomes larger with misaligned crystals with respect to the direction of a higher temperature gradient.

Several factors such as moving heating source power (P), beam scan speed, substrate material temperature (T), and beam spot diameter (d) control the G/R_L ratio^[11], where G is the local temperature gradient. The value of

G is lower with higher values of T . The lower value of G must be recompensed by a lower P -value. Therefore, P must be decreased when T is increased to have columnar growth through the solidification. With an increased scan speed, R_L increases without a significant impact on G , resulting in a lower value of the G/R_L ratio. However, as the higher scan speed causes a smaller melt area with greater temperature gradients, the increased scan speed may increase the G/R_L ratio. A larger energy intensity or a wider beam diameter is inconvenient to work with because of the promptly decreased beam intensity in the area far from the centerline in a single-mode laser with a Gaussian intensity distribution that restricts uniformity in the microstructure. Therefore, when a larger d is unavoidable, P needs to be intensified to confirm enough heat flux for the substrate remelting to continue with epitaxial grain growth. Raising the substrate material temperature using a pre-heating procedure somewhat enables the melting with a larger volume but, at the same time, lowers the processing window.

Moreover, the stability of the solid/liquid boundary is dominated by the thermal and supercooling behavior. Consid-

ering the constitutional supercooling, the instability at the interface is expressed as:

$$\frac{G}{R} > \frac{\delta T}{D} \tag{Eq. 6}$$

where G represents thermal gradient, R is the growth rate, δT is the temperature range for solidification, and D is the diffusion coefficient of solute material in the melt.

To understand the solidification morphology and their structure, a solidification map is designed with G and R , in the form of their product as $G.R$ and ratio as G/R . **Figure 12** describes the influence of G/R and $G.R$ on the solidification structure, where G/R governs the type of solidification pattern and $G.R$ controls the size of the structure.^[10] The solidification structure may be planar, cellular, columnar dendritic, or equiaxed dendritic. Normally, higher G/R ratios result in a planar structure, while lower G/R ratios result in an equiaxed structure. Moreover, the size of these four structures decreases with the larger value of $G.R$ (cooling rate).

The size of the solidification structure can be estimated using the product $G.R$. Therefore, the arm spacing of columnar or equiaxed grains can be measured using the cooling rate or solidification time, which can be stated as^[10]:

$$y = at^{\frac{1}{n}} = b(\epsilon_c)^{-n} \tag{Eq. 7}$$

where t_f is the solidification time, ϵ_c is the cooling rate, and a , b , and n represent material constants that should be identified based on the experimental data.

The mathematical relation depicts that with the slower cooling rate and the extended growth time, coarser dendritic structures are formed. The surface energy of the solidified material may be lowered with the formation of coarse dendrite arms, as the coarse arms have less surface area per unit volume. This is because the slower cooling allows a longer time for growth and forming coarser dendritic arms. On the other hand, a faster cooling rate does not allow a longer time for growth, producing a finer structure.

The driving force, which is required for dendrites to grow properly, comes from undercooling. There is a difference in temperature between the liquidus and the dendrite slant that makes the undercooling temperature, as stated by:^[10]

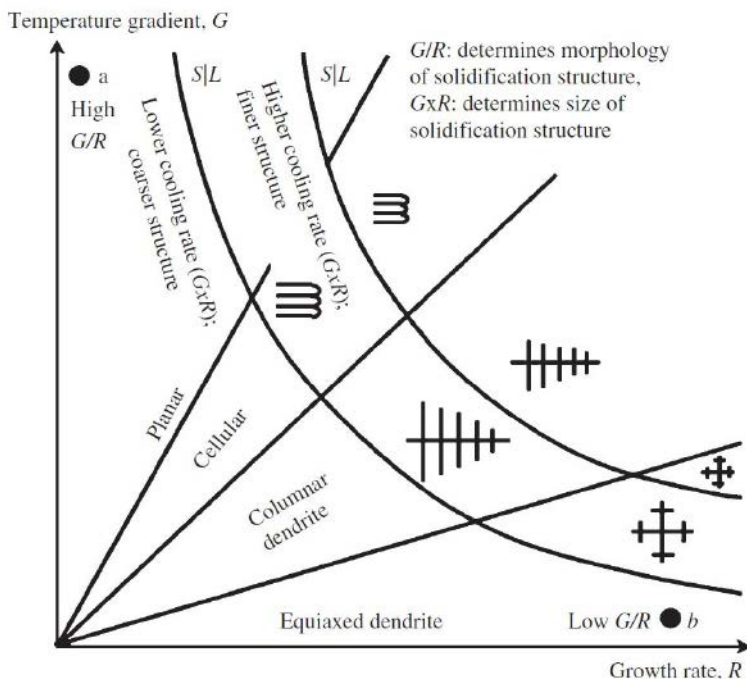


Figure 12: Influence of temperature gradient G and growth rate R on the size and morphology of the solidified structure.^[10]

[Source: Reproduced with permission from John Wiley & Sons Inc.]

$$\Delta T_{tot} = \Delta T_C + \Delta T_T + \Delta T_K + \Delta T_R \quad \text{Eq. 8}$$

where ΔT_C , ΔT_T , ΔT_K , and ΔT_R are the undercooling temperatures accompanied by solute diffusion, thermal diffusion, attachment kinetics, and solid/liquid boundary curvature, respectively.

Through the solidification of most metallic materials, ΔT_T , ΔT_K , and ΔT_R are negligible; hence, the solute diffusion undercooling ΔT_C leads the process. Therefore, different solidification structures, from planar to cellular, columnar dendrite, or equiaxed dendrite, are basically formed because of the supercooling at the solid/liquid interface.

Besides the dendritic structure reported in AM, there may be a considerable amount of precipitates in some precipitation strengthened alloys, such as nickel-based superalloys. This happens because of the very fast cooling in the localized melt area, which creates a non-equilibrium condition where diffusion is limited. Another reason is the inadequate time for the alloying constituents to diffuse back into the solidified structure. Therefore, the concentration of the residual melt increases with alloying elements and promotes eutectic solidification to take place at the end of solidification, resulting in precipitates.

Process Parameters

The solidified microstructure and the phase formations are controlled by the input process parameters. Together with the higher specific energy and the faster deposition rate, the liquid melt will be at a higher temperature for an extended time to lower the temperature gradients. Therefore, the grains are allowed to grow coarsened and mainly equiaxed. On the other hand, the minor specific energy is understood by applying a faster scan speed, and hence no adequate time for the grain growth. Moreover, the geometry of the melt pool becomes narrow at a faster scan speed; therefore, the temperature gradients are higher, resulting in the formation of columnar grains. Layer thickness is also another influencing factor, which depends on additional parameters, e.g., power, speed, specific energy, and powder flow rate, to dominate the microstructure in AM products. When the specific energy is brought down, the energy required per unit area to melt down the powder is lowered. This calls for a need to lower the layer thickness. However, the thicker layer causes slower cooling and results in a coarser microstructure. Therefore, the structural development is complex to layer thickness

because of the dominance of heat conduction through the substrate, which controls the cooling rate and consequent microstructures.

Solidification Temperature Span

Usually, the broader solidification temperature span creates a greater solid/liquid or mushy zone, which is mostly responsible for the solidification cracking, as the liquid cannot allow load. This temperature range is altered by several factors, such as the existence of impurities and some specific alloying elements. Simultaneously, the nearby grain material will be solidified, which then creates a gap with the grain boundary liquid due to thermal stresses. The eutectic temperature range also enhances the extent of the mushy zone.

Gas Interactions

In AM techniques, argon and nitrogen are generally used to offer an inert atmosphere and satisfy the high tolerance criteria. In the case of EB-PBF, a true vacuum in the chamber is required. Helium is also used for shielding during laser DED to enhance temperature-temporal behavior.

The impact of the shielding gas on the quality of metal powders during laser DED, combined with the AM input parameters, plays a major role in the growth of the final structure and properties of the manufactured products. Although nitrogen is a reactive gas, it can be a suitable shielding gas for those materials, which never react with nitrogen.

SOLIDIFICATION DEFECTS

Porosity

Usually, in AM the pore formations are connected with the process input parameters, such as laser power or beam scan speed. The porosities are categorized as powder and process induced.

Three major mechanisms cause porosity in AM products. First, at very high operating powers, melting may be accomplished throughout a keyhole mode.^[11] When the keyholes are not properly developed and stabilized, they can turn into an unstable mode, which then frequently forms and collapses, making voids inside the melt. Second, during the atomization of metallic powder, gas can be trapped inside powder particles, creating microscopic gas pores during the process. Consequently, the powder-caring pores can be transferred to the final fabricated parts. Moreover, gas pores can be generated

because of the potential of gas attraction/solution by the alloy melt. Third, the deficiency in fusion imperfections can result from insufficient infiltration of the upper layer melt into the substrate or the formerly solidified layers. This lack of fusion area is detectable by not melted or partially melted powders nearby the pores.

To understand the mechanisms of defect formations during LPBF, the process window for a known and fixed layer thickness and hatch spacing can be classified into four different zones.^[24] Zone I is termed a “fully dense zone,” which is free from porosity. Zones II and III, which are termed the “over melting zone” and “incomplete melting zone,” respectively, have measurable porosities. The porosities introduced by process input parameters in zone II result from the exceeded energy, whereas those of zone III are caused by inadequate energy flux. Finally, Zone IV, the “overheating zone,” is generated by a very slow scan speed and higher laser power.

Porosities generated by inadequate melting are typically observed near the boundaries, which are geometrically irregular in shape. Their amounts are greatly persuaded by operating parameters, such as laser power, layer thickness, scanning speed, and hatch spacing. In deficient fusion porosity, the top surface of the earlier layer may not be melted to develop a coherent bond due to the unsatisfactory dissipation of laser energy through the powder layers. Another potential reason for the poor fusion porosity is the entrapment of gas bubbles between the layers during processing. These gas bubbles then result in an unsteady scan track with non-uniform evaporation. The distinctive uncertainty of the scan tracks, therefore, causes intermittent failure of the liquid melt adjacent to the vapor cavity and forms periodic voids.

Similar to the process input parameters, the unsteadiness of the scan track and pore formation can be minimized by the proper adjustment of the beam.^[25] There is a chance to release more gas during the slow solidification process, usually at higher energy density or lower scan depth with lower energy densities. Using a pulsed or modulated laser beam, it is possible to regulate the energy indulgence into the powder layer or substrate material, thus manipulating solidified structures, porosity, and other defects. The steadiness of the scan track is significantly impacted by the pulse because the pulse needs to revive the scan track once it fails. The adequate overlap-

ping ratio of the two scan tracks can provide effective removal of porosity formed in early pulse, which eventually minimizes the process-induced cavities. Hence, it is suggested to reduce the lay-off time of the pulse, lower than the solidification time required for the melt. In this situation, it is necessary to use a high duty cycle and a greater extent of overlap area in the melt zone through the pulse transition. During pulsed-wave methods, the consideration of short pulse periods and lower energies is necessary to maintain a small melted area.

Balling

The balling phenomenon is considered the unusual melt pool segregation/breakout that may take place on the surfaces of the laser additive-manufactured parts, especially LPBF. Through the processing, the laser beam scans the surface linearly and the melting occurs along a row of powders, which then creates a constant liquid track similar to a tubular shape. The breakdown of the tube into the spherical-shaped (balling effect) metallic agglomerates drops the surface energy of the melt track until the ultimate equilibrium condition is achieved. The balling effect can result in an intermittent scan track with poor bonding and can be an obstruction to a constant deposition of powder on early-deposited layers. These phenomena can result in porosity or even delamination because of weak interlayers joining together with induced thermal stresses.

In powder-based AM techniques, powder particles absorb energy by the mechanisms of bulk coupling and powder coupling. Initially, a thin layer of distinct powder absorbs energy, influenced by the powder properties. This elevates the temperature on the particle surface, forming a liquid phase through the surface melting of powders. Consequently, the heat flows mostly in the direction of the center of the persisted powders till the steady-state melting temperature is achieved. The volume of liquid formation is influenced by the melting temperature, which is regulated by the laser power and scan speed through line scanning. For example, with a known scan speed and a lower laser power, the solidus temperature drops, forming a smaller volume of liquid melt. This makes a higher viscosity in the liquid-solid mix that, in turn, impedes the liquid flow and particle reordering. This eventually drops the general rheological performance of adjacent and contacting liquid and solid particles. Subsequently, the liquid melt in each exposing spot area is able to combine into a discrete coarsened sphere of approximately the

same size as the laser beam's diameter. In these circumstances, no effective bonding occurs between the adjacent balls since inadequate liquid volume stops the satisfactory growth of continuous connecting metal agglomerates. In fact, the result would be multiple irregular shape discrete solidified zones when one looks at the build plate from the top. In addition, lower laser power is responsible for the inadequate undercooling temperature of the liquid melt. Therefore, the formation of coarsened and irregular dendrite structure in solidified balls generates mechanically weak characteristics, thus undermining the part quality.

When a satisfactory volume of the liquid phase is grown with both greater laser power and scan speed, the melt converts into an incessant tubular melted track because of the short exposure time of laser input on every area underneath the moving beam. But the melt pool track would be in an unsteady state; hence, the surface energy will keep dropping to reach an ultimate equilibrium state. When the scan speed increases, the energy intensity by the laser input drops, which then lowers the surrounding temperature and subsequently the diameter of the tubular melt pool track. Therefore, the melt zone's unsteadiness rises considerably. Under these circumstances, the dropped surface energy promotes the spattering of liquid droplets from the melt pool track surface. As a result, many micrometer-sized spherical spatters are solidified near the sintered surface, ensuing in the balling phenomenon. These irregular shape-solidified zones may cause a manufacturing issue by manifesting the potential of recoater jamming during LPBF.

In a multi-layer deposited sample, the balling effect may be excluded by reducing the powder layer thickness. By applying a deoxidizing agent, oxide films can be satisfactorily eliminated from the melt surface, thereby cleaning the balling zone joining system.

Cracking

a. Solidification Cracking

Solidification cracking takes place at the last step of solidification, where dendrites have become complete grains and are detached by a small volume of liquid known as a grain boundary. The possible reasons for solidification cracking in melted metals are depicted as: (a) temperature range of solidification, (b) volume and dispersion of liquid melt at the end of solidification, (c) the early solidification phase, (d) the surface tension at the grain boundary melt, (e) the grain morphology, (f) the ductil-

ity of the solidifying metal, and (g) the propensity of the weld metal to contract and the amount of restriction. All these aspects are ultimately connected with the metal composition. Here, the first two aspects are influenced by microsegregation, which is controlled by the cooling rate through solidification like the primary phase formation.

b. Intergranular Cracking

Intergranular cracking arises at the grain boundaries during the last step of the solidification, where solidifying and cooling material possesses higher tensile stresses compared to the strength of the solidified metal. Moreover, the substrate material also passes through a thermal cycle developing expansion and contraction on a small scale. Intergranular cracking is worsened by the intensification of thermal power or thickness of the substrate.

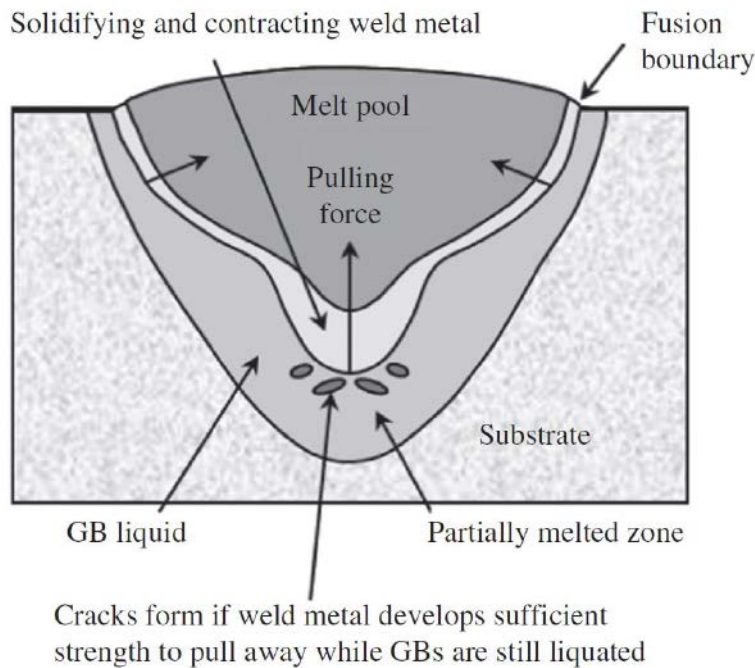
c. Reheat Cracking

Reheat cracking is a common phenomenon in low-grade ferrite steels containing chromium (Cr), molybdenum (Mo), vanadium (V), and tungsten (W). After manufacturing through welding or AM techniques, heat treatment is usually carried out to release stress and minimize the propensity of hydrogen or stress corrosion cracking. However, the major issue is that the cracking may take place in the heat-affected region through reheating.

During AM processes, the temperature in the heat-affected zone close to the fusion line is raised to the austenitizing temperature, where Cr, Mo, and V carbides dissolve into austenite regions. Faster cooling of the heat-affected zone may allow inadequate time to transform carbides, resulting in martensite with supersaturated alloy content. When the reheating is done to release the stress, the alloy content starts to reprecipitate along the high-energy austenite grain boundaries. This stimulates crack formation because of residual thermal stresses.

d. Liquation Cracking

Liquation cracking typically occurs in the mushy zone (MZ) or partially melted zone (PMZ) of the solidified build product, schematically shown in **Figure 13**. The alloy containing low melting temperature carbides results in melting in the PMZ during fast heating, even under the liquidus temperature. When cooling starts to take place, the PMZ undergoes tensile stress because of solidification shrinkage together with the thermal contraction from the solidified layers. In these circumstances, the liquid melt



POST SOLIDIFICATION PHASE TRANSFORMATION

After completing the solidification and cooling far down the solidus temperature, the metal will continue to cool down to room temperature and then endures the solid-state transformation. Reheating of previously deposited layers can again possess phase transformation. Here, the phase transformation that takes place through AM processing is presented for both cases of heat-treatable and non-heat-treatable alloys.

Ferrous Alloys/Steels

Wide varieties of steels have been manufactured through AM. The very usual microstructure of AM-processed austenitic stainless steels is cellular and columnar dendrites. An equiaxed structure is hardly observed because of the higher temperature gradient during the metal AM. The solidified microstructure is mainly cellular, and its size increases with the increase of deposit depth by accumulating heat through the AM techniques. Austenitic steels regularly have a tiny amount of ferrite distant from austenite.

During solidification, solute rejects at the boundary and enhances the intercellular areas with chromium and molybdenum, resulting in ferrite formation. However, the ferrite content drops at a faster cooling rate due to the inadequate time for solute restructuring at higher rates. Austenitic steels show comparatively higher thermal expansion coefficients, thus being susceptible to solidification cracking. For austenitic steels, the propensity to solidification cracking is reduced with the primary δ -ferrite phase, compared to the austenite phase.

Al Alloys

The most promising aspect of fabricating Al products using AM techniques is their higher thermal conductivity, which minimizes thermally produced stresses, as well as the necessity of support structures. Moreover, higher thermal conductivity permits greater processing speeds. The very familiar Al alloys obtainable in AM are the hardenable AlSi10Mg (EN AC-43000) and the eutectic AlSi₁₂ (EN AC-44200). As a high-strength alloy, a hardenable Al–Mg–Sc alloy is recommended by Schmidtke et al.^[26] (AlMg_{4.5}Sc_{0.66}). Al–Sc alloys have received significant attention from the aerospace industry recently due to their high mechanical strength and attractive elongation rate.

Figure 13: The mechanism of liquation cracking in the melt pool area.
Source: Adapted from^[10]. [Reproduced with permission from John Wiley & Sons Inc.]

pool around the grain boundaries or carbides may become the crack initiation locations.

Therefore, the possible reasons for liquation cracking are summarized as (i) wider MZ, formed because of a greater difference between liquidus and solidus temperatures, as observed in nickel-based superalloys, (ii) greater solidification shrinkage due to a larger size melt pool such as Ti-6Al-4V alloy, (iii) greater thermal contraction because of a large coefficient of thermal expansion, as observed in aluminum alloys.

Lamellar Tearing

Lamellar tearing is caused because of the combined effect of localized internal stresses and the lower ductility of the substrate material. The substrate material normally reveals non-metallic inclusions. The tearing is activated by the de-bonding of nonmetallic inclusions such as silicates or sulfides in the substrate metal close to the heat-affected zone, where there is no retrieval of grains or reabsorption of precipitates for the homogenization of microstructure. This region of the substrate also receives greater thermal stresses because of the higher heat input during the AM processes.

In weldable Al alloys, the finer equiaxed grains are known to be less prone to solidification cracking. The equiaxed grains may have distortion by accommodating contraction strains, which make them ductile. The liquid supply and the remedial of initial cracks can also be an additional efficient approach for fine-grained materials. Moreover, finer grain materials with bigger grain boundaries may have less rigorous segregation of low melting solutes. Therefore, the propensity of the weld metal to contract and the level of restraint are the reasons to influence solidification cracking.

The possibility of AM-processed Al alloy parts exhibiting cracking is very robust. This could have been attributed to (i) greater solidification temperature span, (ii) higher coefficient of thermal expansion, and (iii) larger solidification shrinkage^[27]. The laser-processed AM Al alloy also presents liquation and solidification cracks, such as laser-welded Al components. The addition of higher alloying elements in heat-treatable alloys may precipitate lower melting point eutectics, which then create liquation cracks. However, the liquation cracking can be lowered in LPBF manufactured Al alloys by reducing scattered energy concentration from the substrate.

Solidification cracking is barely found in Al alloy manufactured using a continuous-wave Nd:YAG laser; however, the opposite is correct for pulsed-wave Nd:YAG systems. In addition, the heat-treatable 2000 and 6000 Al alloy series are more prone to solidification cracking than the work hardening 5000 alloy series through laser processing.^[25] In Al alloys, the solidification cracking is metallurgically guided by the temperature limit of dendrite consistency and the existing liquid level during cooling. The tendency of solidification cracking enhances with a wider solidification temperature range, which is directly correlated with solidification strains.

In the LPBF process, the non-equilibrium and rapid solidification may result in insufficient diffusion that eventually lowers the liquidus and solidus temperatures. Subsequently, a broader temperature range and larger solidification cracking propensity are usually common in the LPBF process of Al alloys, e.g., 0.8% Si in Al–Si; 1–3% Cu in Al–Cu; 1–1.5% Mg in Al–Mg; and 1% Mg₂Si in Al–Mg–Si alloys^[27]. However, the addition of some alloying constituents with a focus on narrowing down the solidification temperature limit may change the melt pool composition to minimize cracking.

In laser-processed AM, there is an ideal energy density to develop crack-free, entirely dense products. Therefore, the solidification cracking starts at energy densities larger than the ideal value because of the following: (i) lower liquid viscosity, (ii) lengthy liquid period, and (iii) subsequent higher thermal stresses. On the other hand, with lesser energy densities, a disorganized solidification front and a major balling phenomenon may result in crack formation because of the higher unsteadiness of the liquid due to Marangoni convection, nonlinear capillary forces, and inconsistent wetting angles.

The alloying constituents and impurities are segregated along the grain boundaries during the solidification through the microsegregation process, resulting in the liquation layers that also cause the temperature to further cool down. To reduce the sources of stresses and cracks, adequate liquid is needed to seal the cracks and remove the strain generated through the solidification. Thus, crack admittance by strain development competes with crack remedial through refilling by remaining liquid. Although the crack growth rate rises with strains, the replenishing and remedial approach of the remaining liquid is regulated by its fluidity. The eutectic required to avoid cracking differs with composition and cooling rate.

Nickel Alloys/Superalloys

a. Inconel 625

Inconel 625 (IN625) is a Ni-based solid solution strengthening superalloy and is greatly strengthened by Mo and Nb contents.^[28,29] Inconel 625 has applications in aerospace, marine, chemical, and petrochemical industries, possessing superior properties, including strength at elevated temperatures, better creep resistance, excellent fatigue property, resistance to oxidation and corrosion, and accessible processability. However, the microstructure of AM-processed IN625 has austenitic phases, where no carbides and any other phases are recognized. In the laser-processed AM technique, the beam travels very fast (>1,000 mm/s) and makes the solidification time short (<1 ms). The atomic restoration speed ahead of the short period of liquid/solid solidification is greater than the diffusion speed. Therefore, the faster solidification causes the solute atoms to be trapped and creates the well-known “solute trapping.”

b. Inconel 718

Inconel 718 (IN718) is a Ni-based superalloy with higher quantities of Nb, Cr, and Fe.^[30] It has applications in the aerospace and energy/resources industries because of its good oxidation resistance, creep, and mechanical properties at elevated temperatures. IN718 is reinforced by the precipitation of consistent secondary phases. Knowledge of the solidification phenomenon of IN718 is crucial to be familiar with the phase progression in the AM-processed alloys, and the microstructure of Ni-based alloys is essential to improve compositional variants, process mechanisms, and post-processing techniques to reach similar or superior properties of their equivalents manufactured by conventional methods.

Intermetallic compounds like Laves $\text{Ni}_3\text{Nb}-\delta$, and Nb-rich MC are usually found in interdendritic areas or grain boundaries of Ni-based alloys, which undesirably affect the mechanical properties. Laves phase, which occurs in Nb-rich melt with a long-chain structure controlled by Nb segregation and liquid melt distribution, is often found to produce hot cracking. In addition to the cooling rate, Laves phase formation is also influenced by the solidification structure reliant on the proportion of temperature gradient and the growth rate. Smaller dendrite arm spacing with a higher cooling rate and lower G/R ratio helps result in distinct Laves phase particles. In contrast, the larger dendrite arm spacing with a lower cooling rate and higher G/R ratio has a tendency to develop incessantly dispersed larger particles of Laves phase.

c. Stellite

Stellite alloys show better corrosion and wear resistance at a wide variety of interactions and environments in industries, including aerospace, oil and gas, forging, and power production.

The characteristic microstructure of Stellite contains hard carbides distributed through a cobalt-rich solid solution matrix. Stellite 12, which is a hypo-eutectic alloy, forms a solid solution cobalt matrix through solidification. When the temperature drops, the amount of Co in liquid is also lowered and then the eutectic state is attained. The residual liquid reacts with the eutectic structure comprising carbides and a Co-based matrix. Moreover, the alloy possesses blocky eutectic carbides. Laser-processed AM follows faster melting and solidification practice, and the overlapping trends of multiple

tracks and layers will result in remelting of the earlier solidified layers, which may cause divergence in microstructure development.

For Co-based superalloys, the major strengthening mechanisms include solid solution strengthening through the dispersion of Cr, W, and other elements in the Co matrix, whereas M_7C_3 , M_{23}C_6 , and other carbides act as a major function in precipitation strengthening between the dendrite regions. Therefore, the higher hardness of the carbides may enrich the hardness value and wear property of the alloys. For AM-processed Stellite 12, M_7C_3 is the primary carbide, which is in a metastable condition and decomposes to discharge Cr, C, and W elements at higher temperatures and facilitates the formation of M_{23}C_6 and M_6C carbides.

Titanium Alloys

Titanium alloys have vast applications in aerospace, chemistry, ship manufacturing, and other industrial sectors due to their superior properties, e.g., greater strength-to-weight ratio, high corrosion resistance, and compatibility with composite structure in the application of structural parts^[31].

The metallurgy of Ti alloys is directed by the phase transformation that occurs in pure metal at 882 °C (1619 °F). Pure titanium shows an alpha (α) phase (hcp structure) below the temperature and a beta (β) phase (bcc structure) above the temperature.

The primary outcome of alloying additions to titanium is the modification of the conversion temperature and formation of two-phase structures, having both α - and β -phases. Commercially obtainable titanium alloys are categorized based on the impact of α - and β -phases, which consist of (i) α alloys, (ii) near- α , (iii) α - β , (iv) near β , and (v) β alloys. The α alloys are generally not heat treatable and typically weldable; α - β alloys are heat treatable and weldable, with the possibility of losing ductility near the weld area; β alloys are easily heat treatable, mostly weldable, and show higher to medium temperature levels. In a solution-treated state, the alloy possesses superior cold formability. Various types of stabilizing constituents on Ti alloy and their impact on phase transformation are schematically presented in **Figure 14**.

A Stabilizers: These types of components have large solubility in the α -phase, which usually increases the transformation temperature. The effect of α -stabilizing elements on the titanium

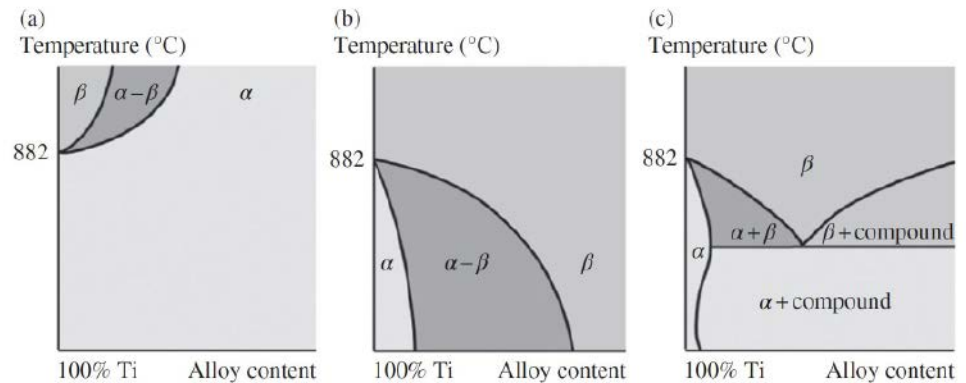


Figure 14: Effect of (a) α -stabilizing, (b) β -isomorphous, and (c) on β -eutectoid elements on the titanium phase diagram.

[Source: openly accessible.]

phase diagram is presented in **Figure 14a**. Very common α stabilizers to Ti alloy are Al, O₂, N₂, or C. The addition of O₂ to pure Ti has the potential to make a variety of grades with higher strength. Al is a commercially used stabilizer, which also acts as the main constituent of many commercial alloys. It can effectively strengthen the α -phase at a higher temperature of about 550 °C (1022 °F). The α -phase can be also reinforced with tin or zirconium, which have substantial solubility equally in the α - and β -phases. They do not prominently affect the transformation temperature and are therefore known as neutral stabilizers.

β Stabilizers: Components that reduce the transformation temperature, easily disperse in and reinforce the β -phase, and show lower α phase solubility are termed β stabilizers. They can be classified into two classes based on their constitutional activities with Ti, β -isomorphous elements (Mo, V, Nb, and Ta), and β -eutectoid elements (Fe, Cr, and Mn, where eutectoids are decomposed as titanium–iron, titanium–chromium, and titanium–manganese).

Variation in the phase composition is a significant basis of microstructural heterogeneity in AM-produced metallic products. For example, in $\alpha + \beta$ titanium alloys (Ti-6Al-4V), usually, three phases are stated, e.g., α phase, β -phase, and α -martensitic phase. Because of the intricate phase transformation methods, it is challenging to precisely calculate the phase composition in AM Ti alloys. The cooling rate and the manufacturing temperature are the two key process parameters to affect the ultimate phase structures in laser or EB-AM-made parts. Therefore, the microstructural differences result from repeated thermal inputs from sequential builds.

Multiple studies have been conducted to shed some light on the effect of faster cooling on the microstructure development in Ti64 alloy by Ahmed and Rack, where improved Jominy and quench test techniques were adopted^[32]. The development of a complete martensitic structure is noticed at cooling rates of 410 and 20 °C/s. This conversion is gradually switched by diffusion-influenced Widmanstätten α -phase at slower cooling rates.

PHASES AFTER POST-PROCESS HEAT TREATMENT

Ferrous Alloys

In laser manufactured 17-4 PH steel, austenite reversion occurs during the aging treatment. The austenite phases in laser-processed AM steel transform to martensite during heat treatment. This is believed to happen due to the stress release, which permits the austenite to transform martensite through post-treatment cooling. Austenite reversion is also common in laser fabricated maraging steel, where during aging, Ni-rich returned austenite shell forms around the retained austenite areas^[33].

Al Alloys

The precipitation-hardened AISi10Mg alloy in the AM process does not show any precipitates because of the rapid solidification, except for some Si segregation near the grain boundaries. After solution treatment, Si starts to form Si particles in the α -Al matrix. The application of water quenching and peak-hardening followed by solution treatment results in globular Si particles with needle-like Mg₂Si precipitates. Therefore, the microstructural anisotropy is diminished through disappearing dendrites, melt pool edges, and heat-affected zones.

Ni Alloys

For IN718, the most commonly applied heat treatments are homogenization or solution aging treatment, which can stimulate the diffusion process through the segregation of some components and dissolve some phases of carbides and Laves in the austenite matrix. Moreover, aging can promote the precipitation of γ' and γ'' elements. After the heat-treatment process, the plate-like δ -Ni₃Nb precipitates form along the grain boundaries, as well as within the grains. However, γ' and γ'' precipitates are very fine to determine with precision.

For cobalt-based superalloys, solid solution and precipitation strengthening are the major reinforcing mechanisms. Cr, W, and other components, which disperse on the cobalt matrix, can act as solid solution strengtheners. M₇C₃ is the major carbides of Stellite 12, which is a metastable phase, fabricated through Laser AM techniques. This carbide phase will decompose to Cr, C, and W components during heat treatment and promote the formation of M₂₃C₆ and M₆C carbides.

Ti Alloys

Ti-6Al-4V alloy possesses excellent stability in strength, ductility, fatigue, and fracture properties, except for the creep property at temperatures above 300 °C. The structural development of this alloy is greatly influenced by heat treatment.

In laser-processed AM techniques, the finer acicular α' -phase in the as-manufactured Ti-6Al4V alloy results in an inadequate outcome through a conventional heat-treatment process. The metastable α' -phase is very fine and contains greater densities of dislocations and twins, which impede the grain growth during heat treatment, directing to a finer $\alpha + \beta$ lamellar structure. During the heat treatment (~400 °C), in the first step, the α -phase starts to nucleate along the boundary of the acicular α -phase, which pushes the vanadium into the boundary of the newly formed α grain. After that, the β -phase forms in the area of higher vanadium content among the α -phase laths. Therefore, the heat-treatment temperature is important to retain the refined microstructure. Moreover, the appropriate temperature and the holding time may relieve the residual stress. Consequently, the stress-relief heat treatment may contribute to two major structural modifications decreasing the dislocation density and the breakdown of α' -phases. The lamellar $\alpha + \beta$ structure, which exists as a colony shape, starts to become coarsen α lamellae

with increasing the heat-treatment temperature. This way, some α grains become globular and reduce morphological anisotropy.

MECHANICAL PROPERTIES

The defects such as porosity influence crack generation and decline in mechanical properties. Therefore, a higher density above 99.5% is usually the first priority for AM technique optimization. The rationale for optimizing parameters to maximize the density by reducing porosities is the fact that the size and distribution of pores have a major impact on mechanical properties.

Hardness

The hardness depends on the cross-sectional area, where with a larger cross-sectional area, the hardness drops due to microstructure coarsening. The basis of this microstructure coarsening is the greater thermal input in a bigger area, which makes a slower cooling process. Therefore, the heterogeneity in hardness depends on the thermal history of the individual layer. Prospective improvement using different process parameters with respect to the cross-sectional area may improve the heterogeneity in hardness.

a. Hardness of AM-Processed Ferrous Alloys

For multi-layer deposited steels, the micro-hardness value drops from the very initial deposited layers, which afterward enhances along the upper layers. This phenomenon is because of the repeated heating of the former layers and letting the time be annealed to some extent. Additionally, this inconsistency is ascribed to the time dependency of the cooling rate in the liquid melt and comparatively the slow solidification rate in the middle area. Therefore, greater hardness values are typically obtained both at the top and bottom of the AM parts in contrast with the central area.

In low alloy steels (41XX series), the content of alloying components, as well as the amount of carbon, controls the phase formation, which eventually affects the hardness values. In high carbon-containing steel, through the rapid cooling in the AM process, hard martensite phases are developed, which contribute to hardness development.

Austenitic stainless steels such as 316 and 316L have a similar chemical composition with an identical dendritic structure. However, a slight change in carbon content ($316L \leq 0.03$ wt.%

C and 316 \leq 0.08 wt.% C) between 316L and 316 shows a significant change in hardness.

b. Hardness of AM-Manufactured Al Alloys

The most familiar Al alloys fabricated through the AM technique contain greater volumes of Si, which stimulate eutectic solidification. The combined effect of higher cooling rates and alloying elements (e.g., Si) promotes the formation of finer secondary arms spacing, which results in higher hardness in AM-manufactured alloys.

Some post-processing techniques may influence the hardness property in AM-processed Al alloys. Previous research has reported that solutionizing and aging treatment may drop the hardness value, compared to the as-deposited condition. This may occur due to the influence of microstructural change caused by solutionizing and aging treatment, which coarsen the Si particles.

On the other hand, HIP, as a post-process technique, also has an impact on the hardness of AM-manufactured alloys. HIP usually results in microstructural coarsening as well as releasing residual stresses, which drop the hardness of products.

c. Hardness of AM-Manufactured Nickel Alloys

The faster cooling rate in AM-processed Ni alloys leads the strengthening elements such as Mo and Nb to remain in the Ni alloy matrix. Therefore, a greater lattice distortion occurs by these point defects, which also enhances the hardness of the AM-fabricated samples compared to the conventional cast alloys. As IN625 is a solid solution-strengthened superalloy, phase transformation occurs through heat treatment. At low-temperature annealing (e.g., 700 °C (1292 °F)), the release of residual stress lowers the hardness. However, annealing between 800 and 900 °C (1472 and 1652 °F) forms δ (Ni₃Nb) precipitate, which improves the hardness. δ is an orthorhombic phase having a greater mismatch with the Ni matrix and thereby develops hardness. However, annealing above 1,000 °C (1832 °F) dissolves δ phases in the Ni matrix and reduces the lattice distortion together with hardness.

d. Hardness of AM-Manufactured Ti Alloys

Generally, the AM-processed Ti-6Al-4V alloy possesses different structural features after various post-processes. For example, LPBF-processed Ti-6Al-4V alloy shows a finer martensitic structure with acicular laths after

stress relieving. In contrast, HIP results in a coarser structure of lamellar α and β .

Ti-6Al-4V alloy endures a phase change from body-centered cubic β phase to a structure comprising hexagonal α -phase and few amounts of β -phase when the temperature is about 1,000 °C (1832 °F). The solid-state transformation may result in measurable structures within grains and, based on the cooling behavior during the conversion of temperature, the α -phase may result in diverse morphology.

Some post-processing treatments, such as heat treatment and annealing, may release residual stress with some coarsening effect of α -phases, which eventually raise the ductility and toughness, compromising the strength and hardness of AM-manufactured Ti-6Al-4V alloy. The precipitation hardening and solid solution strengthening both cause the mechanical property to increase.

Tensile Strength and Static Strength

a. Tensile Behavior of AM-Fabricated Ferrous Alloys

Tensile behavior of the AM-manufactured steel often satisfies the required specifications for technical usage. Formation of finer grains precedes a substantial rise in yield strength and ultimate tensile strength. As for the ductility of the AM samples, a minor amount of porosity results in ductile fracture with elongation values similar to wrought alloys. On the other hand, a greater amount of porosity influences brittle failure, which considerably lowers elongation. The AM-manufactured precipitation strengthening steels are relatively soft, as there is no precipitation formation due to inadequate time for faster solidification. In martensitic grade steels, the amount of retained austenite and austenite reversion phenomenon impacts the tensile properties.

b. Tensile Behavior of AM-Fabricated Al Alloys

The finer grains developed in AM-processed Al alloys promote increased strength in the as-built condition. However, the precipitation strengthens the AM-fabricated AlSi₁₀Mg alloy, which shows similar tensile properties to the solution-strengthened AlSi₁₂ alloy. During heat treatment of AM-fabricated AlSi₁₀Mg alloys, the earlier fine grain becomes coarser, and precipitation formation takes place. The coarse grains deteriorate the tensile strength, whereas precipitates strengthen the alloy. The AM-manufactured scandium-containing alloy aids to retain fine grain structure and also completely coherent precipitates after aging

heat treatment. However, in the AA 2139 (Al–Cu, Mg) alloy, loss of Mg occurs during AM, which afterward lowers the precipitate volume as well as drops the tensile strength.

c. Tensile Properties of AM-Manufactured Ni Alloys

The tensile behavior of AM-fabricated Ni alloys is comparable to the wrought one, while the ductility is low because of the precipitation of γ' and γ'' phases in the austenite matrix, and δ phases around the grain boundaries.

d. Tensile Properties of AM-Manufactured Ti Alloys

In AM, Ti-6Al-4V is the most comprehensively studied group of alloys. As Ti is an appropriate material for different AM techniques, the process input parameters influencing microstructures and tensile behaviors have been considered systematically, specifically for Ti-6Al-4V alloys. The better tensile strength is correlated with the finer martensitic structure resulting from rapid cooling. Finer grains always enhance yield strength and ductility. The deformed hexagonal lattice of α' martensite is stronger compared to lamellar α , which is due to the finer lath width, without reducing the ductility.

Typically, AM-fabricated Ti-6Al-4V alloy has better tensile strength than cast or wrought alloys, i.e., $\alpha + \beta$ alloys, but lower ductility than pure Ti, because of the impeding of the twinning deformation phenomenon.

It is concluded that AM-manufactured Ti-6Al-4V alloy is equivalent to cast or wrought products. It is important to note that the tendency of anisotropy is divergent for tensile strength and ductility using different techniques. The lower ductility of Ti-6Al-4V alloy manufactured using LPBF and laser-directed energy deposition techniques are ascribed to the development of brittle martensite phases. Ductility is the anisotropic property, which is different in the horizontal and vertical direction of the building and can be improved through post-process heat treatment.

Fatigue Behavior of AM-Manufactured Alloys

The fatigue property depends on the isotropic behavior of the AM-fabricated samples. Usually, fatigue strengths are greater in the horizontal built direction than the vertical direction in the LPBF process. The fatigue life of the as-fabricated AM samples is considerably lower than the wrought ones, which is due to the surface roughness and inter-

nal defects influencing the cracks to initiate. The fatigue property of AM products can be enhanced by post-processing heat treatment, hot isostatics pressing, and surface quality improvement. Besides surface features and internal defects, fatigue crack growth also depends on the crystallographic direction of grains that hold the crack tip, the number of grain boundaries around it, and the type of residual core stress. Post-processing like surface grinding and heat treatment may significantly enhance the mechanical properties of AM-fabricated parts to be similar or even superior to conventional counterparts.

a. Factors Influencing Fatigue Behavior in AM

The well-known defects to introduce fatigue cracks in AM components are the pores and voids generated from entrapped gas and/or lack of fusion, as well as inadequate fusion. There is a controversy about the build orientation anisotropy on the mechanical properties of AM products. The difference in thermal profile experienced in different build directions control the morphology of the microstructure, defects, and eventually the ductility.

Tensile residual stresses are disadvantageous to fatigue properties; their impact may be reduced or prevented through suitable process parameters, corrected build direction, or releasing them by applying post-processing heat treatment (PPHT).

b. Fatigue Performance of AM-Manufactured Ferrous Alloys

The fatigue property of 316L alloy is influenced by its monotonic strength. The building orientation shows a significant impact on the fatigue life of 17-4 PH steel. Usually, the horizontally built samples show higher fatigue properties because of the structural configuration along the loading direction. However, in vertical samples, defects are detrimental as they create stress accumulation during loading.

The fatigue life of ferrous alloys is influenced by the alloying element and the post-processing techniques. Moreover, PPHT can expand fatigue life through the recovery of ductility and toughness of the alloy.

c. Fatigue Behavior of AM-Fabricated Al Alloys

Although Al alloys have different physical properties than ferrous and Ti alloys, in the areas of thermal conductivity, surface reflectivity, and melt viscosity, the AM-fabricated proper-

ties are comparable. For example, in eutectic AlSi12 and AlSi10Mg alloys, the faster cooling rate develops a finer lamellar dendritic network of eutectic phases. The formation of strengthening phases of Mg₂Si as well as the distribution of Si particles in the Al matrix contributes to the tensile strength of the AM alloy compared to the conventional sand-cast or die-cast alloys. Throughout the plastic deformation, the dendrite structure acts as load-bearing elements by breaking through the dendritic arms, followed by the ultimate delamination of the Al matrix. The rapid cooling rate results in the growth of residual pores and eventually forms initial cracks at vital pores. Therefore, the joining of several cracks causes a rapid fracture while dropping the ductility.

The application of heat treatment usually reduces residual porosity, and thereby fatigue inconsistency. In high cycle fatigue (HCF), the fatigue property is influenced by the resistance to the crack origination rather than growth. Materials performance is connected to the fatigue scheme under consideration. Materials that have an improved tensile strength are stronger in the low cycle fatigue scheme, which is different from HCF.

d. Fatigue Property of AM-Manufactured Nickel Alloys

Wrought IN718 contains δ phases, whereas the AM-fabricated IN718 comprises Laves phases. It is known that the wrought IN718 shows a better fatigue crack resistance than the AM-processed IN718 because of the absence of the detrimental Laves phase.

e. Fatigue Behavior of Additive-Manufactured Ti Alloy

A comparison of the fatigue property with the wrought alloy specifies that AM-manufactured alloys have a shorter fatigue life. It is already identified that the fatigue property of AM alloy is greatly influenced by internal defects, which perform as micro-notches and result in stress accumulation. The application of post-processing treatment is important to remove or shrink pores to a far smaller size, which makes them unable to influence fatigue behavior.

REFERENCES

- [1] J. Dawes, R. Bowerman, and R. Trepleton, "Introduction to the additive manufacturing powder metallurgy supply chain," *Johnson Matthey Technol. Rev.*, vol. 59, no. 3, pp. 243–256, 2015, doi: <https://doi.org/10.1595/205651315X688686>.
- [2] G. Egger, P. E. Gygax, R. Glardon, and N. P. Karapatis, "Optimization of powder layer density in selective laser sintering," *10th Solid Free. Fabr. Symp.*, pp. 255–263, 1999.
- [3] W. E. Frazier, "Metal additive manufacturing: A review," *J. Mater. Eng. Perform.* 2014, doi: <https://doi.org/10.1007/s11665-014-0958-z>.
- [4] Y. J. Liang, X. Cheng, and H. M. Wang, "A new microsegregation model for rapid solidification multicomponent alloys and its application to single-crystal nickel-base superalloys of laser rapid directional solidification," *Acta Mater.*, vol. 118, pp. 17–27, 2016, doi: <https://doi.org/10.1016/j.actamat.2016.07.008>.
- [5] B. Cantor, W. T. Kim, B. P. Bewlay, and A. G. Gilen, "Microstructure – cooling rate correlations in meltspun alloys," *J. Mater. Sci.*, vol. 26, no. 5, pp. 1266–1276, 1991, doi: <https://doi.org/10.1007/BF00544465>.
- [6] D. D. Gu, W. Meiners, K. Wissenbach, and R. Poprawe, "Laser additive manufacturing of metallic components: Materials, processes and mechanisms," *Int. Mater. Rev.*, vol. 57, no. 3, pp. 133–164, 2012, doi: <https://doi.org/10.1179/1743280411Y.0000000014>.
- [7] A. Y. Uzan, Y. Kozak, Y. Korin, I. Harary, H. Mehling, and G. Ziskind, "A novel multi-dimensional model for solidification process with supercooling," *Int. J. Heat Mass Transf.*, vol. 106, pp. 91–102, 2017, doi: <https://doi.org/10.1016/j.ijheatmasstransfer.2016.10.046>.
- [8] W. Kurz and D. Fisher, *Fundamentals of solidification*, Trans Tech Publications, Switzerland, Germany, UK, USA, 1986.
- [9] M. E. Glicksman, "Principles of solidification: An introduction to modern casting and crystal growth concepts," no. 2, Springer, New York, pp. 1–520, 2011, doi: <https://doi.org/10.1007/978-1-4419-7344-3>.
- [10] S. Kou, *Metallurgy, Welding Metallurgy*, 2nd edition, vol. 822, no. 1–3, John Wiley & Sons, 2003.
- [11] T. DebRoy et al., "Additive manufacturing of metallic components – Process, structure and properties," *Prog. Mater. Sci.*, vol. 92, pp. 112–224, 2018, doi: <https://doi.org/10.1016/j.pmatsci.2017.10.001>.
- [12] H. Zhao, "Microstructure Heterogeneity in Additive Manufactured Ti-6Al-4V," Thesis, 2017.
- [13] W. Callister and D. Rethwisch, *Materials science and engineering: an introduction*, 8th edition, vol. 94, John Wiley & Sons, Inc, 2007.

- [14] S. Das, "Physical aspects of process control in selective laser sintering of metals," *Adv. Eng. Mater.*, vol. 5, no. 10, pp. 701–711, 2003, doi: <https://doi.org/10.1002/adem.200310099>.
- [15] D. A. Porter and K. E. Easterling, "Phase transformations in metals and alloys, 3rd edition," CRC Press, p. 138, 2014, doi: <https://doi.org/10.1146/annurev.ms.03.080173.001551>.
- [16] A. Basak and S. Das, "Epitaxy and microstructure evolution in metal additive manufacturing," *Annu. Rev. Mater. Res.*, vol. 46, no. 1, pp. 125–149, 2016, doi: <https://doi.org/10.1146/annurev-matsci-070115-031728>.
- [17] S. A. David and J. M. Vitek, "Correlation between solidification parameters and weld microstructures," *Int. Mater. Rev.*, vol. 34, no. 1, pp. 213–245, 1989, doi: <https://doi.org/10.1179/imr.1989.34.1.213>.
- [18] M. Garibaldi, I. Ashcroft, M. Simonelli, and R. Hague, "Metallurgy of high-silicon steel parts produced using selective laser melting," *Acta Mater.*, vol. 110, pp. 207–216, 2016, doi: <https://doi.org/10.1016/j.actamat.2016.03.037>.
- [19] A. Yadollahi, N. Shamsaei, S. M. Thompson, and D. W. Seely, "Effects of process time interval and heat treatment on the mechanical and microstructural properties of direct laser deposited 316L stainless steel," *Mater. Sci. Eng. A*, vol. 644, pp. 171–183, 2015, doi: <https://doi.org/10.1016/j.msea.2015.07.056>.
- [20] X. Zhao, L. Liu, and J. Zhang, "Investigation of grain competitive growth during directional solidification of single-crystal nickel-based superalloys," *Appl. Phys. A Mater. Sci. Process.*, vol. 120, no. 2, pp. 793–800, 2015, doi: <https://doi.org/10.1007/s00339-015-9290-1>.
- [21] T. Wang, Y. Y. Zhu, S. Q. Zhang, H. B. Tang, and H. M. Wang, "Grain morphology evolution behavior of titanium alloy components during laser melting deposition additive manufacturing," *J. Alloys Compd.*, vol. 632, pp. 505–513, 2015, doi: <https://doi.org/10.1016/j.jallcom.2015.01.256>.
- [22] L. Thijs, M. L. Montero Sistiaga, R. Wauthle, Q. Xie, J. P. Kruth, and J. Van Humbeeck, "Strong morphological and crystallographic texture and resulting yield strength anisotropy in selective laser melted tantalum," *Acta Mater.*, vol. 61, no. 12, pp. 4657–4668, 2013, doi: <https://doi.org/10.1016/j.actamat.2013.04.036>.
- [23] A. Weisheit, A. Gasser, G. Backes, T. Jambor, N. Pirch, K. Wissenbach, *Direct laser cladding, current status and future scope of application*. In: Majumdar J., Manna I. (eds) *Laser-assisted fabrication of materials*. Springer series in materials science, vol 161, Springer, Berlin, Heidelberg, 2013. https://doi.org/10.1007/978-3-642-28359-8_5. pp. 221–240.
- [24] H. Gong, K. Rafi, H. Gu, T. Starr, and B. Stucker, "Analysis of defect generation in Ti-6Al-4V parts made using powder bed fusion additive manufacturing processes," *Addit. Manuf.*, vol. 1, pp. 87–98, 2014, doi: <https://doi.org/10.1016/j.addma.2014.08.002>.
- [25] M. Pastor, H. Zhao, and T. Debroy, "Pore formation during continuous wave Nd:YAG laser welding of aluminium for automotive applications," *Weld. Int.*, vol. 15, no. 4, pp. 275–281, 2001, doi: <https://doi.org/10.1080/09507110109549355>.
- [26] K. Schmidtke, F. Palm, A. Hawkins, and C. Emmelmann, "Process and mechanical properties: Applicability of a scandium modified Al-alloy for laser additive manufacturing," *Phys. Procedia*, 2011, vol. 12, no. PART 1, pp. 369–374, doi: <https://doi.org/10.1016/j.phpro.2011.03.047>.
- [27] X. Cao, W. Wallace, J. P. Immarigeon, and C. Poon, "Research and progress in laser welding of wrought aluminum alloys. II. Metallurgical microstructures, defects, and mechanical properties," *Mater. Manuf. Process.*, vol. 18, no. 1, pp. 23–49, 2003, doi: <https://doi.org/10.1081/AMP-120017587>.
- [28] C. P. Paul, P. Ganesh, S. K. Mishra, P. Bhargava, J. Negi, and A. K. Nath, "Investigating laser rapid manufacturing for Inconel-625 components," *Opt. Laser Technol.*, vol. 39, no. 4, pp. 800–805, 2007, doi: <https://doi.org/10.1016/j.optlas-tec.2006.01.008>.
- [29] V. Shankar, K. Bhanu Sankara Rao, and S. Mannan, "Microstructure and mechanical properties of Inconel 625 superalloy," *J. Nucl. Mater.*, vol. 288, no. 2, pp. 222–232, 2001, doi: [https://doi.org/10.1016/S0022-3115\(00\)00723-6](https://doi.org/10.1016/S0022-3115(00)00723-6).
- [30] B. Farber et al., "Correlation of mechanical properties to microstructure in Metal Laser Sintering Inconel 718," *Mater. Sci. Eng. A*, vol. 712, pp. 539–547, 2018, doi: <https://doi.org/10.1016/j.msea.2017.11.125>.
- [31] G. C. Li, J. Li, X. J. Tian, X. Cheng, B. He, and H. M. Wang, "Microstructure and properties of a novel titanium alloy Ti-6Al-2V-1.5Mo-0.5Zr-0.3Si manufactured by laser additive manufacturing," *Mater. Sci. Eng. A*, vol. 684, pp. 233–238, 2017, doi: <https://doi.org/10.1016/j.msea.2016.11.084>.
- [32] T. Ahmed and H. J. Rack, "Phase transformations during cooling in $\alpha+\beta$ titanium alloys," *Mater. Sci. Eng. A*, vol. 243, no. 1–2, pp. 206–211, 1998, doi: [https://doi.org/10.1016/S0921-5093\(97\)00802-2](https://doi.org/10.1016/S0921-5093(97)00802-2).
- [33] E. A. Jäggle, P. P. Choi, J. Van Humbeeck, and D. Raabe, "Precipitation and austenite reversion behavior of a maraging steel produced by selective laser melting," *J. Mater. Res.*, vol. 29, pp. 2072–2079, 2014, doi: <https://doi.org/10.1557/jmr.2014.204>.

03 Material Parameter Measurement in EVIDENT Microscopy Software Solutions – PRECiV

SUMMARY

Additive manufacturing (AM) and 3D printing are novel manufacturing processes that build metallic or non-metallic parts by adding material, layer by layer, based on computer-aided design models. Evident's PRECiV™ software offers flexible solutions for additive manufacturing quality assurance. With a guided workflow for different measurement tasks, PRECiV image analysis software provides easy-to-use, reliable solutions to conduct complex analyses according to international standards in the field of material qualification and evaluation.

For example, with the Porosity solution, it is possible to measure different porosity-related parameters that help to quickly identify whether the material meets quality requirements. In addition, PRECiV software provides both intercept and planimetric measurements of the grain size structure of AM pieces. Moreover, monitoring the solidification time in titanium or aluminum alloys is a key factor in improved mechanical properties (such as tensile strength and elongation). The locally different energy input on the surface during the additive manufacturing process often causes grains in the material to grow unevenly. This can cause dendrites, a tree-like branching structure. The dendrite arm spacing (DAS) is directly connected to the solidification time. With a known DAS provided by PRECiV software and a specific material-dependent constant, it is easy to calculate the solidification time and tailor the final quality of parts.

Additive manufacturing and 3D printing have been used as standard terms to indicate a novel manufacturing process that builds a metallic or non-metallic part by adding material, layer by layer, based on a computer-aided design (CAD) model. The three-dimensional CAD model is sliced vertically into several two-dimensional sections. These two-dimensional layers will be used as a path for powerful energy sources, which could be welding torches, electron beams or lasers to melt the material onto each other, either wire or metal powder, to form the final component.

PRECiV offers flexible solutions that can be used for additive manufacturing quality assurance. With a guided workflow for different measurement tasks PRECiV provides easy-to-use and highly reliable solutions to conduct complex analysis according to international standards (ISO, ASTM, JIS, DIN) in the field of material qualification and evaluation (Metal, Ceramics, Coatings, Weldments, Aluminum alloys, Cast Iron ...). Analysis is possible on live or already recorded images. As the used measuring conditions can be saved, it is easy to recall them at a later stage. Storing the measurement conditions increases the reproducibility of the results. If one has several images of the same type that need to be measured,

the workflow provides batch processing. This improves the statistical measurement data.

POROSITY

Additive manufacturing techniques using optimized process parameters can build parts with relative density higher than 99.8%. Even when using optimized process parameters and operational conditions, it is reported that there is an uncontrolled and unavoidable percentage of porosity in additive manufactured parts. Porosity directly influences the mechanical properties and operational performance of the part.

There are at least three sources for porosity in AM manufactured parts: gas porosity, lack-of-fusion, and keyholing.

With the "Porosity" solution in PRECiV image analysis software, it is possible to measure different porosity-related parameters. Porosity describes any void or hole found in a material. The morphology of pores in terms of their size, shape, surface constituents, location and frequency, help to ascertain the defect's origin.

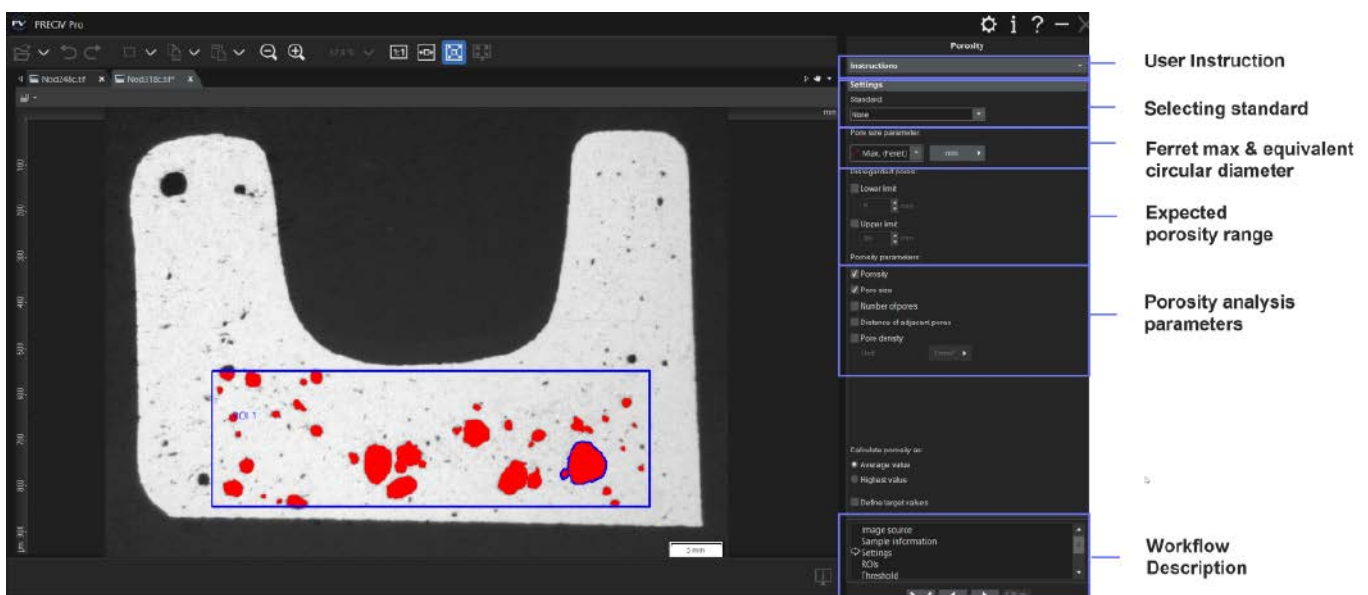
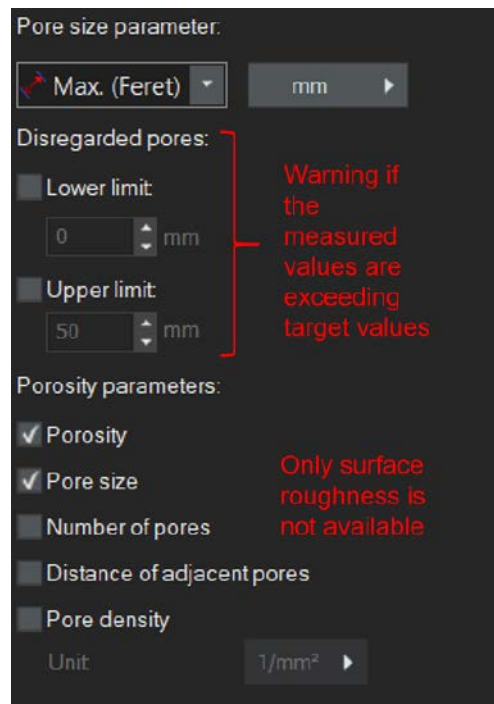


Figure 1: Workflow-based pore analysis in a region of interest (ROI)

Pore analysis parameters

With a threshold-based measurement of pore content per ROI, the software calculates the following parameters: Porosity, Pore Size, Number of pores, Distance of adjacent pores and the pore density. The setting of limits helps to quickly identify whether the material meets quality requirements.



GRAINS

Additive manufacturing will melt material layers onto each other with powerful energy sources to form the final product. Melting processes change the microstructure of the material used.

For metals and ceramics, grain size is one of the most significant metallographic measurements as it directly affects mechanical properties. Common grain size measurements include grains per unit area/volume, average diameter or grain size number. Grain size number can be calculated or compared to standardized grain size charts.

To make the grain boundaries visible, sample preparation must be carried out. Grinding, polishing and etching are necessary steps for good results.

PRECiV software provides both intercept and planimetric measurements, covering the latest version of the most commonly used standards in academic and industrial environments.

Since these are materials solutions of the software, a guided workflow with batch processing is available as well as the ability to save the settings. However, it is also possible to manually intervene if necessary, e.g. if intersections of the measuring grid with the grain boundaries are not correctly detected or are falsified by inclusions within the grains.

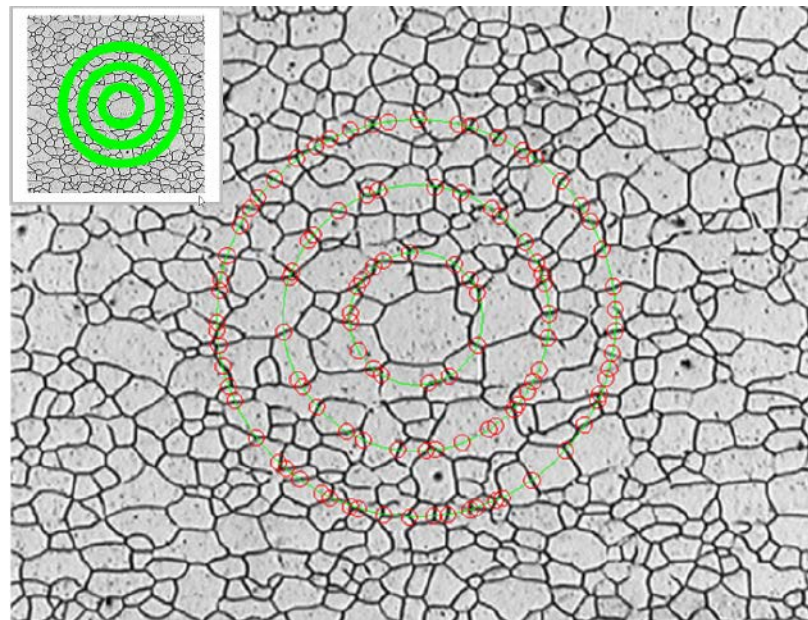
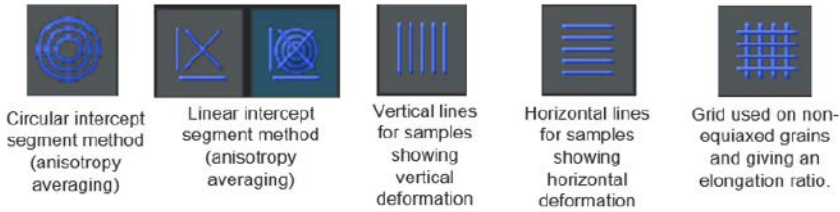


Figure 2: Example grains intercept measurement with circular measuring grid

In the "Grains Intercept" solution different measuring grids help to consider the geometry of the micro structure like the following examples show:

Due to the averaging over the pattern length, the software solution delivers precise results (+/- 0.1 G). The precision is always a function of the number of images measured – batch processing can speed up the analysis. In addition, various available patterns make it possible to obtain the elongation value for non-equiaxed microstructures. So for Grains Intercept measurements, PRECiV provides a single value G, the mean intercept length, the average number of intercepts, the number of intercepts per unit length (1/mm) and if measured, the value for the elongation.



In contrast to the intercept method, "Grains Planimetric" refers to the entire area of grains. After reconstruction, the grain boundaries—the area of all grains—is calculated. Originally, a test circle was used for this purpose, as the first analyses were carried out in the eyepieces of the microscope.

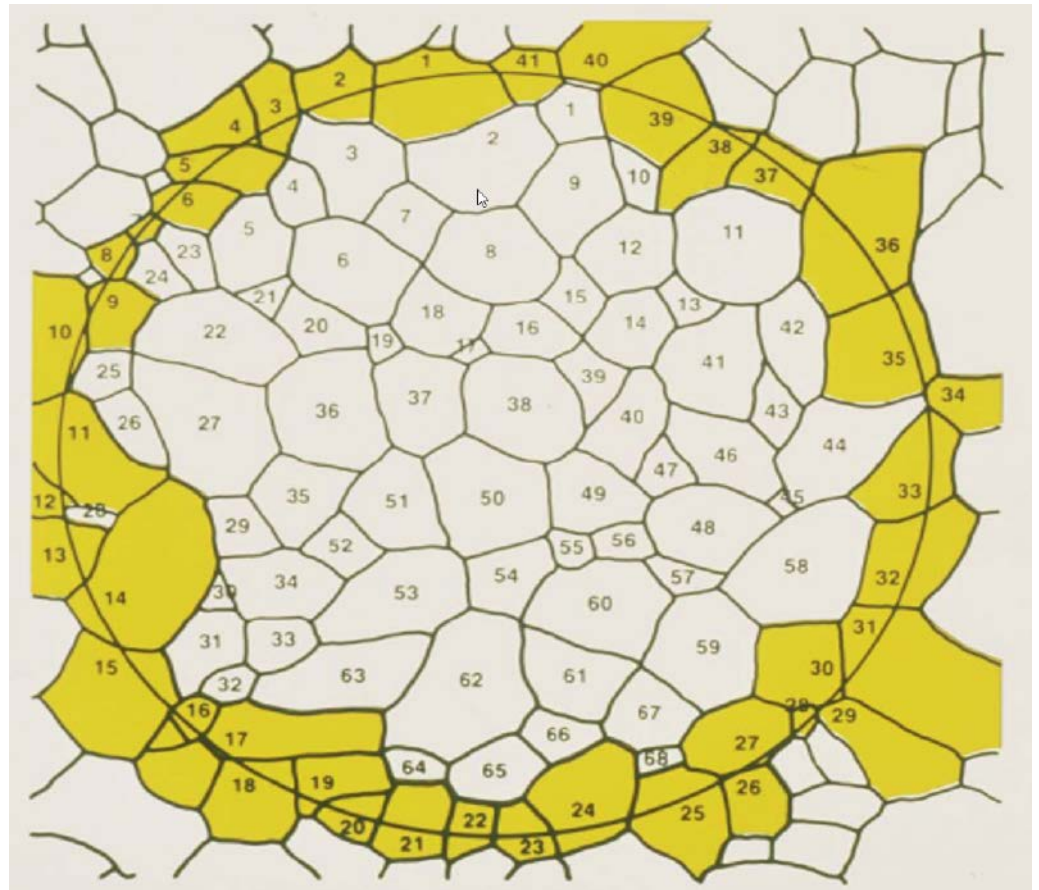
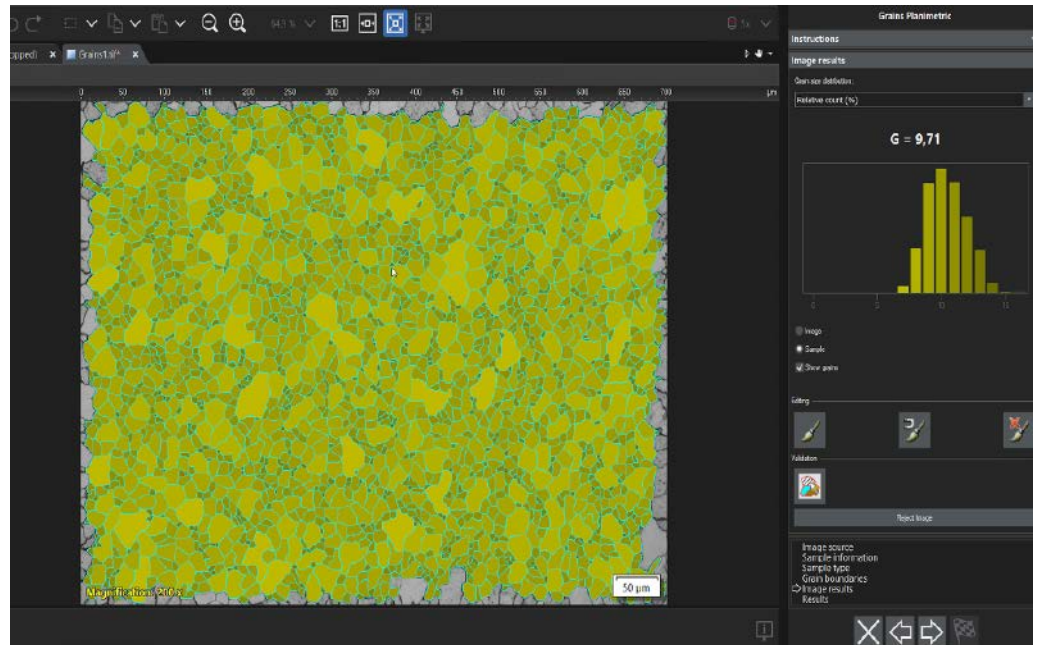


Figure 3: Historical test circle for planimetric analysis

Figure 4: Grains Planimetric analysis in PRECIV



In our modern world, we can leave that approach and use the entire image instead.

The advantage of the planimetric method is that it provides the full information about all grains, the grain size distribution on the evaluated area and geometric information like elongation. A second phase can be considered and evaluated.

DENDRITE ARM SPACING

Dendrite arm spacing is an interesting method. Originally known from light metals like Aluminum and Magnesium, it is an important analysis method for additive manufactured materials. Due to the locally different energy input on the surface during manufacturing process, the grains in the mate-

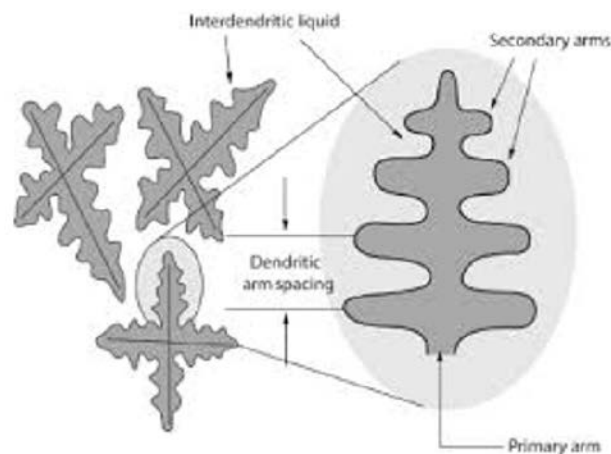
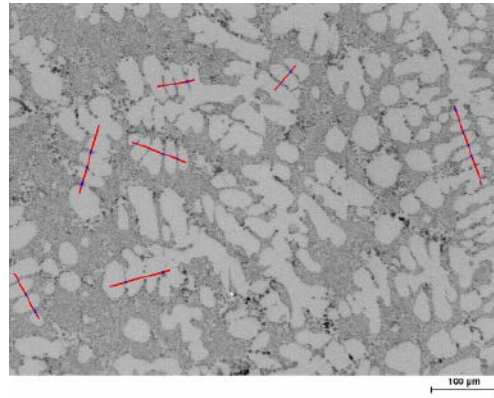


Figure 5: Crystal growth in dendrite form

Figure 6: Manual measurement of Dendrite Arm Spacing



rial often grow unevenly. That results in dendrites, a tree-like branching structure.

The monitoring of the solidification time in such alloys is a key factor to improved mechanical properties (like tensile strength and elongation). The Dendrite Arm Spacing is directly connected to the solidification time.

With a known Dendrite Arm Spacing (DAS) and a specific material-dependent constant it is easy to calculate the solidification time.

A precondition for a dendrite arm spacing measurement is that the dendrites differ from the rest of the sample, for example by contrast. In this case, dendrites will have different intensity values from the rest of the sample, making automatic analysis of the image possible. Setting thresholds for detecting the dendrites is a good and quick solution in this case. On the other hand, a manual measurement can be conducted.

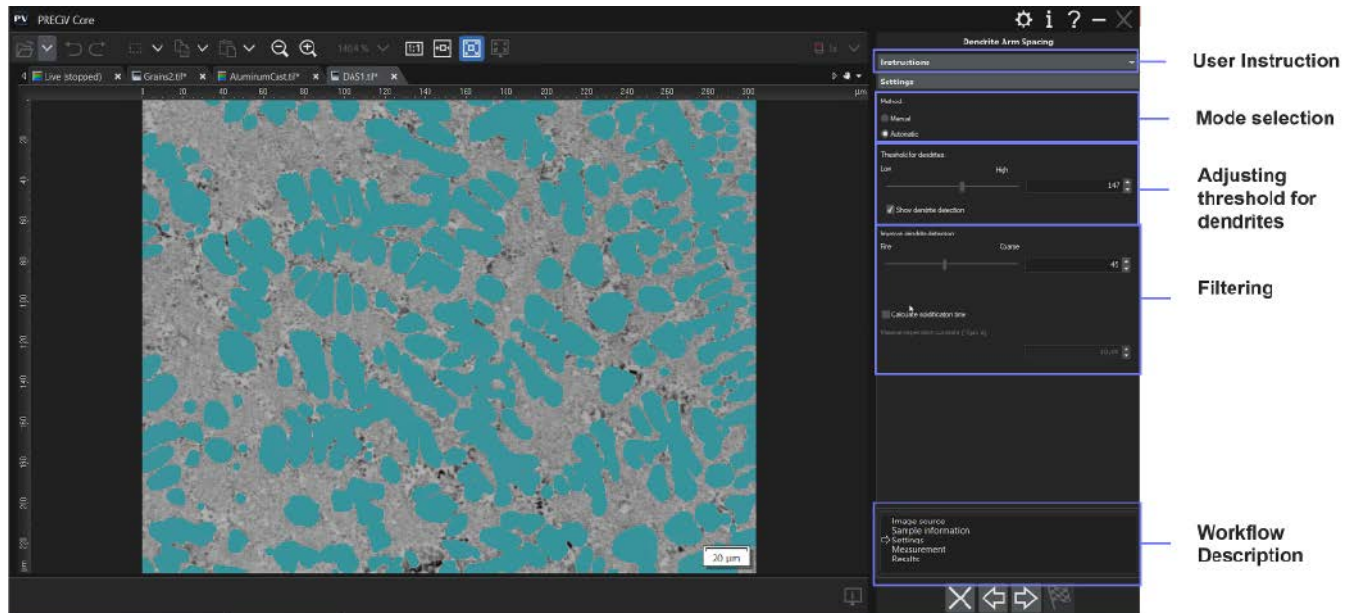


Figure 7: Automatic measurement using threshold inside of the guided workflow